THE GEOLOGICAL SOCIETY OF AMERICA®

Textural and geochemical window into the IDDP-1 rhyolitic melt, Krafla, Iceland, and its reaction to drilling

E. Saubin[1,†], B. Kennedy[1], H. Tuffen[2], A.R.L. Nichols[1], M. Villeneuve[1,8], I. Bindeman[3], A. Mortensen[4], C.I. Schipper[5], F.B. Wadsworth[6], T. Watson[1], and R. Zierenberg[7]

[1]*School of Earth and Environment, University of Canterbury, Christchurch, New Zealand*
[2]*Lancaster Environment Centre, Lancaster University, Lancaster, UK*
[3]*Department of Earth Sciences, University of Oregon, Eugene, Oregon 97403, USA and Mineralogical Museum, Moscow, Russia*
[4]*Landsvirkjun National Power Company of Iceland, Reykjavik, Iceland*
[5]*School of Geography, Environment and Earth Sciences, Victoria University of Wellington, New Zealand*
[6]*Department of Earth Sciences, Lower Mountjoy, Durham University, Durham, DH1 3LE, UK*
[7]*Earth and Planetary Sciences, University of California, Davis, California 95616, USA*
[8]*Chair for Subsurface Engineering, Montanuniversität Leoben, Austria*

ABSTRACT

The unexpected intersection of rhyolitic magma and retrieval of quenched glass particles at the Iceland Deep Drilling Project-1 geothermal well in 2009 at Krafla, Iceland, provide unprecedented opportunities to characterize the genesis, storage, and behavior of subsurface silicic magma. In this study, we analyzed the complete time series of glass particles retrieved after magma was intersected, in terms of distribution, chemistry, and vesicle textures.

Detailed analysis of the particles revealed them to represent bimodal rhyolitic magma compositions and textures. Early-retrieved clear vesicular glass has higher SiO_2, crystal, and vesicle contents than later-retrieved dense brown glass. The vesicle size and distribution of the brown glass also reveal several vesicle populations. The glass particles vary in δD from −120‰ to −80‰ and have dissolved water contents spanning 1.3–2 wt%, although the majority of glass particles exhibit a narrower range. Vesicular textures indicate that volatile overpressure release predominantly occurred prior to late-stage magma ascent, and we infer that vesiculation occurred in response to drilling-induced decompression. The textures and chemistry of the rhyolitic glasses are consistent with variable partial melting of host felsite. The drilling recovery sequence indicates that the clear magma (lower degree partial melt) overlays the brown magma (higher degree partial melt). The isotopes and water species support high temperature hydration of these partial melts by a mixed meteoric and magmatic composition fluid. The textural evidence for partial melting and lack of crystallization imply that magma production is ongoing, and the growing magma body thus has a high potential for geothermal energy extraction.

In summary, transfer of heat and fluids into felsite triggered variable degrees of felsite partial melting and produced a hydrated rhyolite magma with chemical and textural heterogeneities that were then enhanced by drilling perturbations. Such partial melting could occur extensively in the crust above magma chambers, where complex intrusive systems can form and supply the heat and fluids required to re-melt the host rock. Our findings emphasize the need for higher resolution geophysical monitoring of restless calderas both for hazard assessment and geothermal prospecting. We also provide insight into how shallow silicic magma reacts to drilling, which could be key to future exploration of the use of magma bodies in geothermal energy.

INTRODUCTION

Context

Our knowledge of the behavior of subsurface magma is mostly built on observations and analysis of fossil intrusions or pyroclasts together with experimental approaches. These are valuable, but they do not directly represent in situ magma bodies. An unprecedented opportunity to characterize an in situ active magma reservoir arose in 2009 with the drilling of a geothermal well at Krafla.

Krafla is a central volcano with an 8–10 km diameter caldera located on the northern rift zone of Iceland (Fig. 1). Its most recent eruptive episode, between 1975 and 1984, involved basaltic fissure eruptions and repeated episodes of rifting, intrusion, and ground deformation (Björnsson, 1985). Early seismic velocity surveying and shear wave shadowing indicated the presence of a potential 0.7–1.8-km-thick magma body at around 3 km depth (Brandsdóttir et al., 1997) and extending <3 km N-S and <10 km E-W (gray blobs on Fig. 1). Past eruptive activity indicates that Krafla is basalt-dominated (Sæmundsson, 1991; Mortensen et al., 2015; Kennedy et al., 2018, and references therein); however, partial melting of basaltic crust has generated rhyolite magma, and a mixed rhyolite-basalt eruption is thought to have been responsible for most of the caldera's subsidence (Marsh et al., 1991; Jónasson, 1994; Rooyakkers et al., 2020). Two other eruptive phases have created rhyolitic domes and ridges both within the caldera and at its margins (Jónasson, 1994; Tuffen and Castro, 2009). Later geophysical investigation confirmed another low seismic velocity zone at 2–3 km depth beneath Krafla's Víti crater that was inferred from earthquake and active seismic data (Schuler et al., 2015). The data indicated that it may correspond to a shallow rhyolitic intrusion or superheated steam. The complex bimodal magmatic system extends between 2 km and 8 km depth and is the heat source of a ~40 km^2 hydrothermal system that hosts a geothermal power station that has been operating since 1977 (Einarsson, 1978; Ármannsson et al., 2014; Mortensen et al., 2014).

The first Iceland Deep Drilling Project-1 (IDDP-1) well was completed in 2009 at Krafla

†elodie.saubin@yahoo.fr.

GSA Bulletin; https://doi.org/10.1130/B35598.1; 9 figures; 1 table; 1 supplemental file.

For permission to copy, contact editing@geosociety.org
© 2021 Geological Society of America

Downloaded from http://pubs.geoscienceworld.org/gsa/gsabulletin/article-pdf/doi/10.1130/B35598.1/5211391/b35598.pdf
by Univ of California Davis Serials Dept, Robert A. Zierenberg

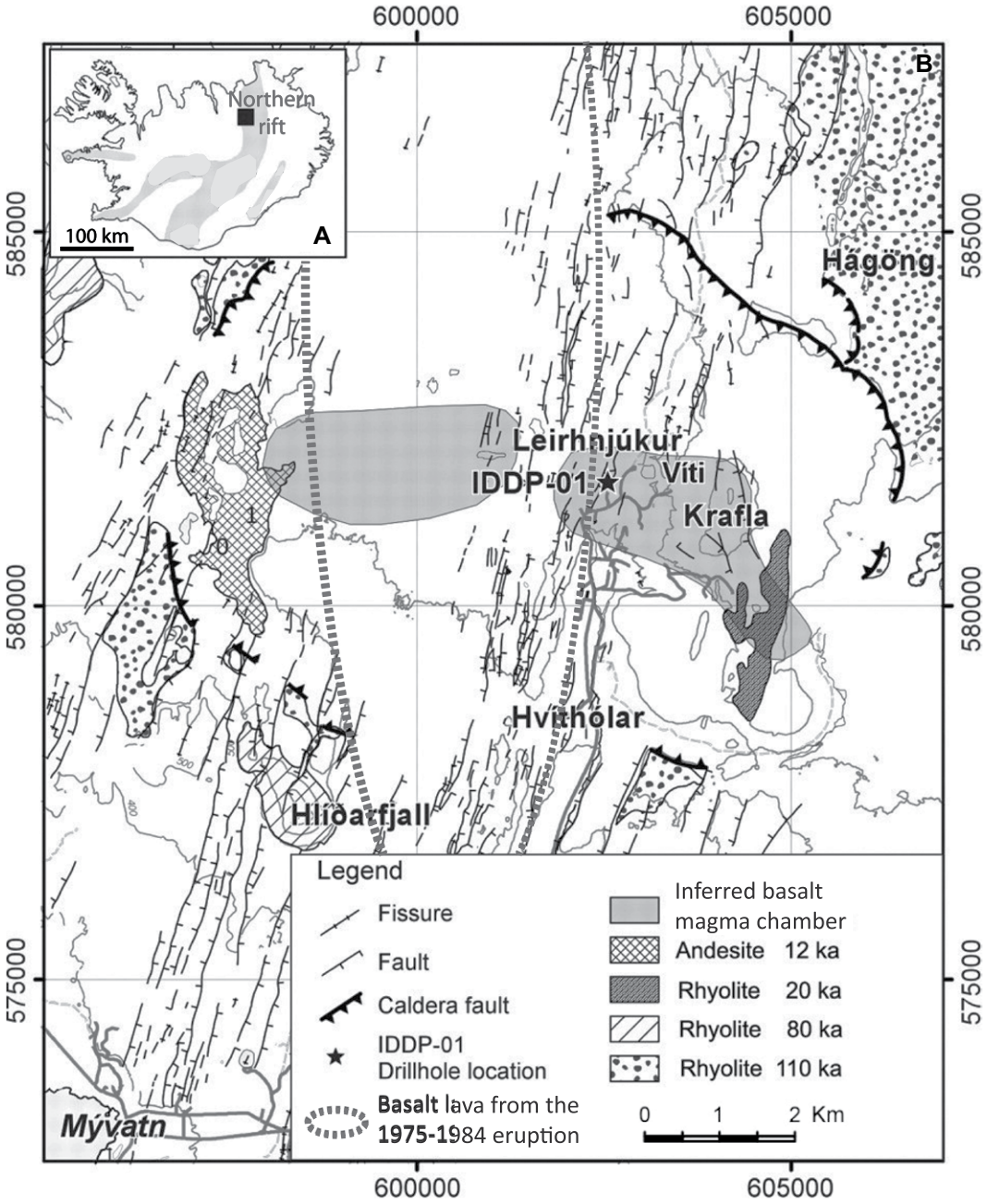

Figure 1. Map shows Krafla caldera and geothermal field and was adapted from Elders et al. (2011). (A) Krafla location on the north Iceland rift zone. (B) Location of the Iceland Deep Drilling Project-1 (IDDP-1) well and surface projection of the ~4-km-deep basalt magma chamber inferred on the basis of S-wave shadows (Einarsson, 1978).

with the aim of reaching supercritical fluids at the margins of the deep basaltic magma chamber. Prior to drilling, geophysical data, including the distribution of seismicity and resistivity, were used to choose the site and depth for the borehole as the best target for supercritical fluids with no evidence of shallow magma (Friðleifsson et al., 2014; Fig. 1). However, drilling had to be stopped at a depth of only 2104 mbs (meters below surface) when the drill bit repeatedly became stuck (Friðleifsson et al., 2010). Drilling below 2104 mbs was attempted three times; two sidetracks were attempted in addition to the original hole. These sticking events occurred on 21 April, 8 June, and 24 June 2009, corresponding to intervals of 50 days and 16 days between events (comprising withdrawing attempts, sidetracking, and re-drilling; Friðleifsson et al., 2010; Pálsson et al., 2014). On the third approach, the drill bit had been carefully pulled up 9 m above the well bottom but was pushed upwards for 4 min and became stuck. Ultimately, the lowest ~20 m of the hole became plugged. The retrieval of fresh silicic glass particles in returned drill cuttings revealed the cause of drilling difficulties (ISOR Iceland Geosurvey, 2009; Friðleifsson et al., 2010). The modeled temperatures and the weight on bit (WOB) and torque reaction of the drill string (Friðleifsson et al., 2010; Pálsson et al., 2014) indicated three encounters with mobile liquid magma at a depth of ~2103–2104 mbs. Despite these difficulties, IDDP-1 became the hottest (452 °C at the well head; Friðleifsson et al., 2013) and one of the most productive geothermal wells in the world until it was abandoned in 2012 following complications arising from a collapse of the well casing in 2010 (Ingason et al., 2014). IDDP-1 is now renowned as an example of a super-hot geothermal well

Downloaded from http://pubs.geoscienceworld.org/gsa/gsabulletin/article-pdf/doi/10.1130/B35598.1/5211391/b35598.pdf
by Univ of California Davis Serials Dept, Robert A. Zierenberg

that intersected magma. Among the few other inferred occurrences of deep magma encountered worldwide—in Hawaii in 2005 (Teplow et al., 2009) and in Kenya since 2011 (Mbia et al., 2015)—the retrieval of quenched glass from IDDP-1 makes it an unprecedented target for characterizing in situ rhyolite magma from an active magma reservoir.

As the location of the IDDP-1 magma body is well known, and magma intersection did not induce any eruptive events, the Krafla Magma Testbed project (KMT; http://kmt.is) now aims to drill back into the magma and create a global testbed for monitoring subsurface magma and assessing volcanic hazards (Eichelberger, 2019). The success of any new "magma wells" crucially depends on having a sound understanding of magma reaction to drilling and magma behavior at the reservoir margins. Processes of magma emplacement/formation, reservoir size, and relationship with host rocks are also key parameters that impact overlying fluid reservoirs and their geothermal potential (e.g., Bostick and Pawlewicz, 1984). In this study, we provide detailed textural and compositional data on silicic glass from IDDP-1, for the complete time-series of glass particle retrieval, constrained by the timeline of drilling events. Our detailed analysis includes the novel combination of componentry and vesicle size distribution, the use of 3-D X-ray computed tomography, and thermogravimetric analyses. We discuss the physical reaction of the magma to drilling and examine the scenarios for magma storage and the partial melting at the reservoir margins. Key evidence includes the relation between glass texture (vesicularity, crystallinity, color) and composition (major elements, isotopes, and volatile content) as well as the componentry of the retrieved particles.

Terminology

The samples retrieved from the IDDP-1 well are called "cuttings" in drilling literature but are referred to here as "particles" for all types of lithologies. The particles coming from the quenched magma are called "glass." The terms "granophyre" and "felsite" are used interchangeably in published literature, but here we exclusively use the term felsite for this host rock lithology. The time of particles' retrieval from the well is referred to as "retrieval time." Because glass particles contain crystals, we consider the encountered melted rhyolite as a "magma" rather than a pure "melt." The oxides and ferromagnesian mineral phases are grouped into the term "ferromagnesian crystallinity," here comprising titanomagnetite, pigeonite, and augite. We finally refer to the IDDP-1 rhyolite magma as a "magma body" or "magma reservoir" rather than using the interpretive term of "intrusion" that has been commonly used in the literature.

Previous Work on the IDDP-1 Rhyolite

The lithologies encountered by the well remain poorly constrained by age and lateral extent, but down hole geophysical logging indicates that felsite is the most likely host rock for the magma encountered by the well (Mortensen et al., 2014). The holocrystalline felsite, a fine-grained plutonic equivalent of rhyolite, is mechanically weaker than the overlying basalts and potentially easier to intrude (Eggertsson, 2019). Its mineral assemblage has been shown to consist of plagioclase, pigeonite, augite, titanomagnetite, quartz, and alkali feldspar (Elders et al., 2011; Zierenberg et al., 2013). Interstitial fresh glass in felsite particles has only been identified in particles retrieved from the precise interval where magma is inferred: at 2103 mbs. Previous studies of the IDDP-1 glass have revealed much about their texture and chemistry. Recovered glass particles were rhyolitic, and all contained identical mineral phases with few (<3 vol%) and small (mostly <100 μm) phenocrysts of plagioclase, pigeonite, augite, and titanomagnetite (Elders et al., 2011; Zierenberg et al., 2013; Masotta et al., 2018). A few glass particles have higher crystal content, which additionally included quartz and alkali feldspar with resorbing textures. Previously analyzed glasses were silica-rich (75.1 wt% SiO_2) with low TiO_2 (0.3 wt%). Glass volatile contents averaged 1.77 wt% H_2O and 85 ppm CO_2 but varied with glass texture (vesicularity, crystallinity, and color; Trewick, 2015) and retrieval time (Watson, 2018) within the range of 1.43–1.91 wt% H_2O. Average isotopic compositions of $\delta^{18}O$, 3.1‰, and δD, −121‰, with δD overlapping that of local hydrothermal epidote, suggested that the source of the rhyolitic magma had been hydrothermally altered (Elders et al., 2011; Pope, 2011; Seligman and Bindeman, 2011). The hydrothermal water causing the alteration was inferred to have had a meteoric isotopic signature consistent with the meteoric water-recharged Krafla geothermal system. There has been no evidence of magma interaction with drilling fluids (Elders et al., 2011; Schiffman et al., 2014), and the speciation of total H_2O (high OH/H_2O_m ratios of 1.46–2.53; Zierenberg et al., 2013) confirmed there was no late hydration of the glass during drilling. In addition, crystal textures and thermobarometric calculations revealed identical crystallization conditions in the rhyolite glass and host felsite, with partial melting, mixing, and incorporation of crystals from the felsite into the crystal-poor rhyolite magma having occurred (Zierenberg et al., 2013; Masotta et al., 2018). Similar bulk compositions of the rhyolite glass and the felsite particles show that the rhyolite magma could have formed by partial melting of the host felsite, which was itself derived from partial melting of hydrothermally altered basalt (Elders et al., 2011). Felsite partial melting experiments at 950 °C reproduced the end-member glass compositions, with rhyolite glass and felsite compositions that represent sub-liquidus and sub-solidus states of the same magma, respectively (Masotta et al., 2018). The last magmatic activity at Krafla was the 1975–1984 Krafla Fires basaltic eruption, which involved sustained heat input from shallow basaltic intrusions. This event could have enhanced magma generation below the IDDP-1 drill site (Elders et al., 2011; Masotta et al., 2018).

Previous work published on the IDDP-1 particles primarily focused on samples retrieved at only three time intervals (16:15, 17:00, and 8:00–13:00 on 24–25 June 2009). Here, we widen this sample set to include particles recovered over a longer time window (>9 h). We analyze the componentry of all types of retrieved particles and specifically examine the vesicle textures in glass using vesicle size distributions to characterize degassing through nucleation, growth, and coalescence (e.g., Sparks, 1978; Rust et al., 2003; Okumura et al., 2006; Hamada et al., 2010; Shea et al., 2010) and bubble number density to calculate decompression rates (Toramaru, 2006). We complement published major element chemistry and $\delta^{18}O$ and δD values of IDDP-1 glass particles with an expanded data set of these elements to further explore the magma genesis and degassing dynamics (Taylor et al., 1983; Newman et al., 1988; Zhang, 1999; Taylor, 2001; Pope et al., 2014; Castro et al., 2014).

METHODS

The analytical protocol is summarized in Figure 2. Detailed study was restricted to the glass particles that represent the quenched magma we wish to understand. Particles were analyzed in terms of texture (vesicle number density, size, shape and distribution, crystallinity) and composition (major elements, water content, hydrogen isotopes). Interpretation of the results is set within the context of previous work on IDDP-1 particles and the context of drilling using sample retrieval times with the timeline of evolving drilling parameters and operations (e.g., fluid circulation, bit advance, and string pull-out). This timeline is derived from raw data and drilling reports provided by Landsvirkjun, the owner and operator of Krafla geothermal power plant, and main funder of the IDDP-1 operation.

Downloaded from http://pubs.geoscienceworld.org/gsa/gsabulletin/article-pdf/doi/10.1130/B35598.1/5211391/b35598.pdf
by Univ of California Davis Serials Dept, Robert A. Zierenberg

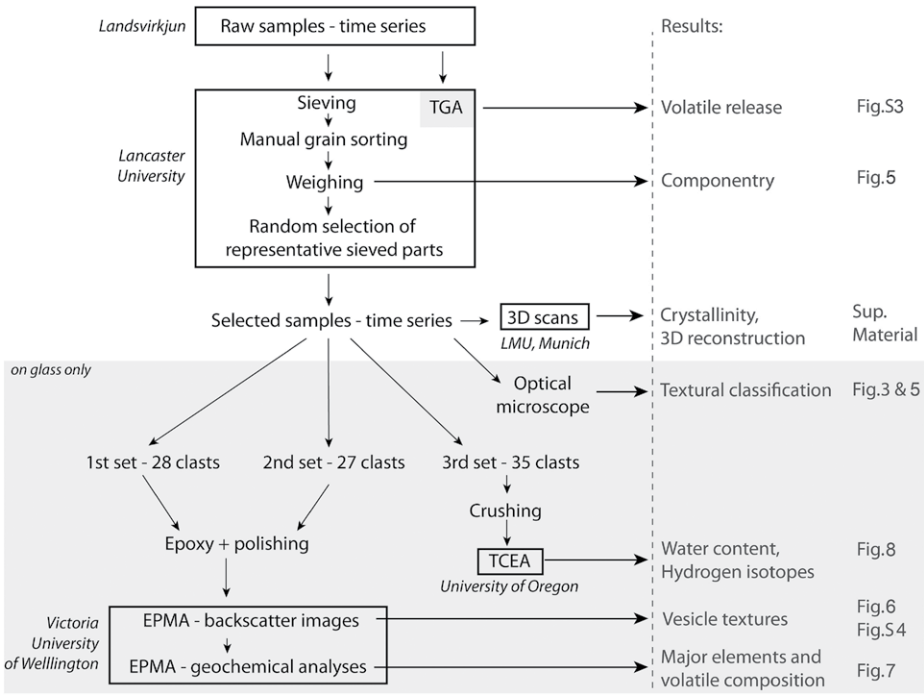

Figure 2. Protocol followed for data collection of Iceland Deep Drilling Project-1 particles conducted at the University of Canterbury, New Zealand, unless otherwise mentioned. Analyses in the gray area were performed on selected glass particles only.

The drilling data are provided in Figure S1[1] and span the initial magma intersection to the end of the cutting retrieval.

IDDP-1 Cutting Componentry

Particles were recovered from 22 bulk samples retrieved at regular intervals in the IDDP-1 well from 15:15 on 24 June 2009–00:50 on 25 June 2009. Sampling started two hours after the magma was first intersected (at 13:27), when the drill bit was stuck at a constant depth after having been pushed up by the magma (Fig. S1). The particles represent a sample from the deepest drilling depth (2104 mbs). Bulk samples were sieved into four grain size fractions. The largest particles (1–2 mm and 2–4 mm) were sorted into four categories using optical inspection of their characteristics: fresh glass derived from the intersected magma, crystalline felsite with no apparent interstitial glass, glassy felsite that visibly contains high interstitial glass fraction, and drilling contaminants (lost circulation material [LCM], here nut shells and mica flakes). Each category was weighed to determine componentry (particle distribution) evolution over time. From the sieved fractions, 5–10 particles were randomly selected from each category and subjected to further analysis (gray shaded region in Fig. 2). Samples taken at 15:15 and 15:30 were not considered for analysis as the particle size was too small to be manually sorted.

IDDP-1 Rhyolite Glass

We analyzed a total of 251 glassy particles from the 1–2 mm and 2–4 mm size fractions with 5–35 particles per retrieval time. These particles were sorted into textural sub-categories using an optical microscope.

Vesicularity of each particle was first qualitatively estimated by visually comparing the apparent fraction of vesicle area with a reference chart displaying a range of vesicle area fractions. The results were used for initial particle classification. The vesicularity of 26 particles with various textures was subsequently calculated using the ImageJ software on backscatter electron (BSE) images collected with a JEOL JXA-8230 SuperProbe at Victoria University of Wellington (VUW). For each particle, the average vesicularity was calculated from one to three images, and internal variations within single particles were recorded. Visual estimates of vesicularity are in good agreement with the calculated values, although three particles were incorrectly classified by initial analysis, resulting in a ~12% error in classification (Fig. S2; see footnote 1). Among other parameters considered for textural classification were vesicle shape, size, elongation direction, and spatial distribution, but we ultimately based the final classification on the two criteria showing the most obvious variations and the lowest human bias uncertainty: color (clear, brown, or black glass) and 2-D vesicularity as an area percentage (non-vesicular, <1%, 1%–3%, and >3% vesicularity). We use relative vesicularities to refer to the <1% and 1%–3% categories as poorly vesicular and the >3% category "vesicular." Most particles in this category have 3%–6% vesicularity, and a few have up to ~15%. These relative descriptors are appropriate for this sample set, but we recognize that all IDDP-1 glass particles would be considered "poorly vesicular" relative to conventional pyroclast classification schemes. Representative particles and examples of classified glass particles are shown in Figure 3.

To reduce bias caused by human color perception, color identification was conducted by comparison with reference particles of distinct clear and brown colors. As brown glass can appear clear around vesicles, color identification was conducted, when possible, on vesicle-free portions of particle borders. Similarly, the impact of particle size (a very thin brown glass can appear clear) was addressed by comparison with similar-sized reference particles. There are additionally some rare black glass particles that have an oxidized surface, which suggests they could be altered clear or brown glass.

BSE images were used to characterize vesicle textures and proportions. Vesicle properties were analyzed in 25 glass particles that span the time series, the range of vesicularities, and the full range of vesicular textures (distribution, size, shape, orientation). The protocol is similar to that described in Shea et al. (2010): each particle was imaged at four magnifications with a minimum of 11 images per particle distributed as in Figure 3B. The images were processed with Adobe Photoshop™ to select, redraw, and attribute a grayscale color to vesicles (Fig. S4C–S4D; see footnote 1) prior to analysis with FOAMS software, which provides the volume fraction size distribution corrected from 2-D pictures (Shea et al., 2010). The aspect ratio of vesicles (short axis divided by long axis) is used to describe their elongation, where a value of 1 indicates equant and round vesicles. However, textural classification using both microscope observations and BSE images did not allow for the identification of any systematic relationship between vesicle orientations and spatial

[1]Supplemental Material. Figures S1–S4 and Digital Material S5-1–S5-4. Please visit https://doi.org/10.1130/GSAB.S.13249994 to access the supplemental material, and contact editing@geosociety.org with any questions.

Downloaded from http://pubs.geoscienceworld.org/gsa/gsabulletin/article-pdf/doi/10.1130/B35598.1/5211391/b35598.pdf
by Univ of California Davis Serials Dept, Robert A. Zierenberg

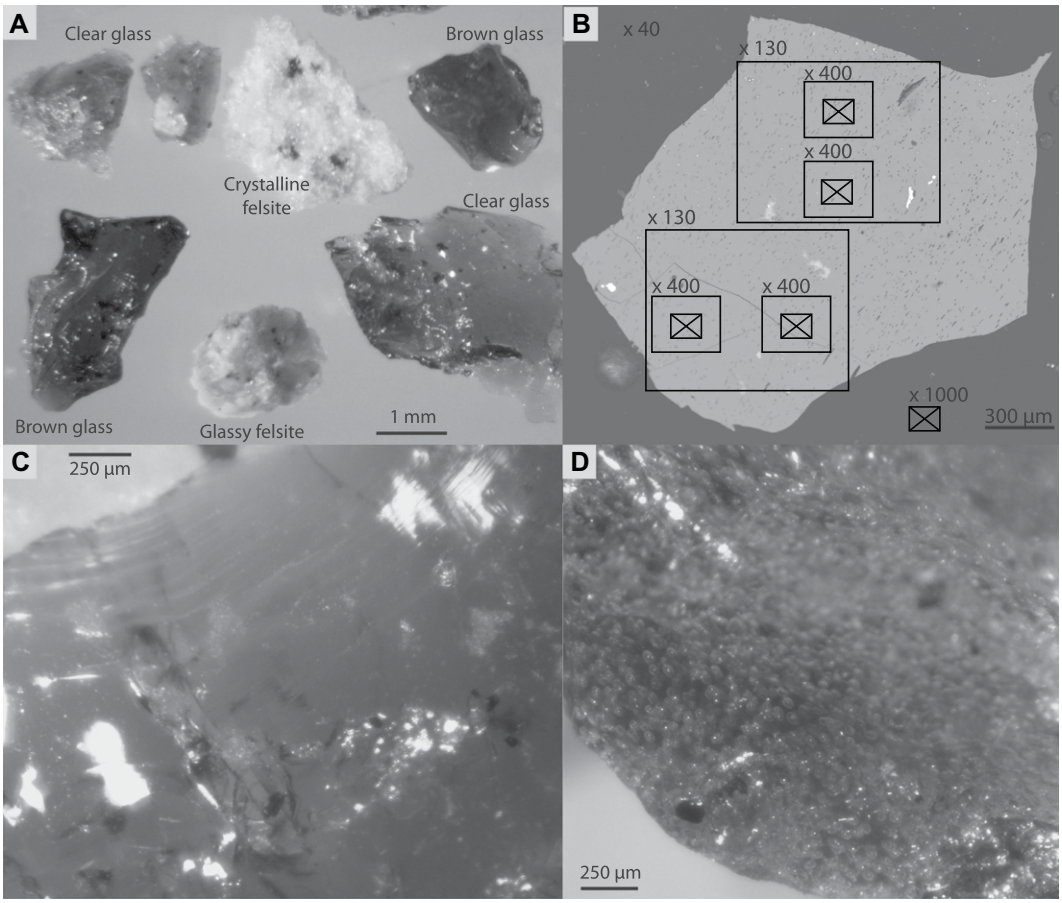

Figure 3. Iceland Deep Drilling Project-1 particles are shown. (A) Particles from the 18.30 sample (1–2 mm size range). (B) Backscatter image of clear, vesicular glass (>3% vesicularity) from the 18.00 sample. Method of image selection for FOAMS analyses: overview picture is at 40× magnification, two areas are at 130×, in which two zones are randomly selected at 400× and 1000×, providing a minimum of 11 images per particle. (C) Brown, non-vesicular glass, 2–4 mm in diameter, from the 19.30 sample. (D) Brown, vesicular glass (>3% vesicularity), 2–4 mm in diameter, from the 17.00 sample.

distributions. The diversity of vesticles shape is illustrated in Figure 4.

Three-dimensional renderings of nine particles were reconstructed by X-ray tomography using a GE Phoenix Nanotom E laboratory scanner operating at 80–90 kV and 120–250 nA and using a 0.1–0.2-mm-thick aluminum filter to reduce beam hardening. These conditions resulted in a voxel edge length of 1.7–2.2 μm. The filter back projection reconstruction was performed using the GE proprietary software, and visual three-dimensional reconstruction was performed with the Drishti software (Limaye, 2012). Samples imaged include one clear glass, one brown glass, one crystalline felsite, and one glassy felsite particle; the digital representations highlight the crystal phases, vesicles, and shapes of the particles (Supplementary Material S5; see footnote 1). A part of the image stacks was used for crystallinity calculation using ImageJ 3-D object counter plugins according to the software's memory limitation (176 images for clear glass, brown glass, and crystalline felsite and 145 images for the glassy felsite). Quartz and feldspar were not readily discriminated from glass, so crystallinity calculations were limited to ferromagnesian and oxide phases only. We collectively refer to these phases as ferromagnesian crystallinity and recognize that they do not represent the full crystal population. The X-ray tomography images are used in this study to support our textural observations because the long scan times meant that we could not analyze sufficient particle numbers to be representative of the drilling time-series.

Two sample sets were analyzed separately for chemical compositions and isotopic ratios (Fig. 2). Major elements and volatile species (S, F, and Cl) in glasses were determined by electron probe micro-analysis (EPMA) using JEOL JXA-8230 at Victoria University of Wellington, set at 15 kV, 8.0 nA for major elements and 15 kV, 60 nA for volatiles. The beam was defocused to give a beam diameter of 10 μm; peak and background count times were 30 s and 15 s, respectively, for most elements with shorter counting times (10/5 s) for Na, longer (60/30 s) for S and Cl, and longer (120/60 s) for F (see Schipper et al., 2019, for details). Natural and synthetic compounds (Jarosewich et al., 1980; Jochum et al., 2005; Zhang et al., 2016) were used to calibrate the measurements, and analytical drift and reproducibility were checked by interspersing glass standard analyses among the sample measurements. These analyses were also performed on a third sample set previously used for volatile measurement (Watson, 2018). We conducted five spot analyses on each particle. Water contents and hydrogen isotope ratios were measured with a Thermal Conversion Elemental Analyzer (TCEA-MAT253) at the University of Oregon. Analytical errors are ± 2 δD and ± 0.03 wt% H_2O (e.g., Martin et al., 2017; Hudak and Bindeman, 2018). All data are reported on the Vienna standard mean ocean water (VSMOW) scale based on concurrently run standards of both liquid waters and solid.

Individual glass particles from the 17:00 bulk sample were used to examine the origin of the H_2O using thermogravimetric/mass spectrometry analysis (TGA-MS) conducted using a Netzsch STA449C Jupiter system at Lancaster University that was hyphenated to a Hiden HPR20 mass spectrometer (Applegarth et al., 2013). Temperature uncertainty is <2 °C. Powdered glass was heated to 1250 °C at 10 °C/min. The sample was then cooled to 25 °C at 10 °C/min and subjected to a second identical heating. The TGA curves presented in the Supplementary Material (Fig. S3; see footnote 1) are buoyancy corrected via subtraction of the second heating

Downloaded from http://pubs.geoscienceworld.org/gsa/gsabulletin/article-pdf/doi/10.1130/B35598.1/5211391/b35598.pdf
by Univ of California Davis Serials Dept, Robert A. Zierenberg

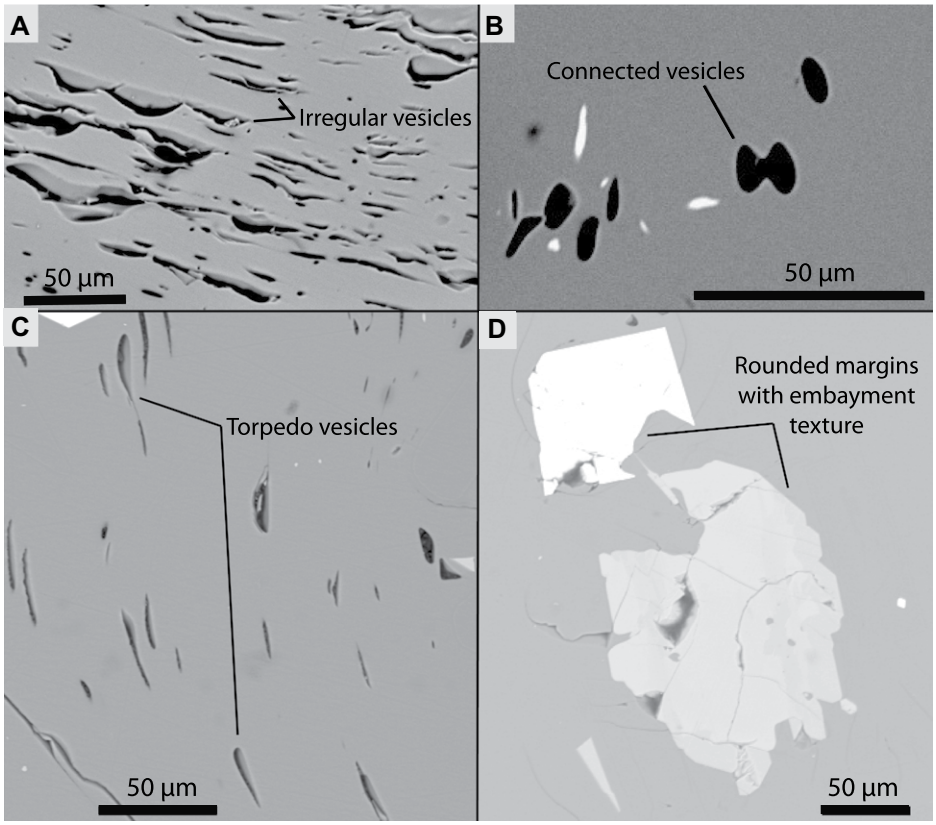

Figure 4. Vesicles textures are shown in backscatter electron (BSE) images. (A) Glassy felsite particle sampled at 16:30 has >3% vesicularity. We interpret the irregular and elongated vesicle shape to be caused by vesicle collapse. (B) Coalescence texture in clear glass with <1% vesicles sampled at 16:00. (C) Moderately elongated vesicles with torpedo shapes in a clear glass sampled at 23:00 have <3% vesicularity. (D) Embayment textures of crystals, in a clear glass particle sampled at 16:00, suggest resorption. The crystal edges are rounded.

segment from the first (e.g., Applegarth et al., 2013), and dTGA curves are calculated from corrected TGA values.

RESULTS

We separate the results into clear and brown glass categories, from large scale to smaller scale analyses (i.e., componentry to texture to composition), and relate them to the sample retrieval time where relevant.

Componentry

The proportion of glassy felsite (felsite with up to ~30% interstitial glass content; Masotta et al., 2018) over the time series shows similar temporal component variations to that of crystalline felsite (with no apparent interstitial glass). As both have similar mineralogy and texture, they are paired in a single felsite category. Componentry analysis over the retrieval time (Fig. 5) shows that rhyolite glass accounts for almost 100 wt% of the retrieved particles over most of the time series (Fig. 5A). However, the felsite content was higher during the first two hours (up to 70 wt%). This period was followed by an abrupt decrease around 17:15, and the proportion of drilling contaminants increased at the end of retrieval up to 60 wt% after 23:00. Temporal variations in glass color (clear, brown, or black) are presented in Figure 5B, where brown glass is most abundant. The initially high clear glass proportion abruptly drops from ~45% to ~15% (in number of same-sized particles calculated from a subset of raw samples, Fig. 2) at around 17:15. Black glass forms an irregular and minor component (<4% particles) throughout the whole series and is thus dismissed from further analysis. Up to 60% of the glass is vesicular until 17:15, when poorly vesicular glass suddenly becomes predominant (Fig. 5C); vesicular glass then constitutes <20% of the distribution in number of particles. The proportion of clear glass correlates with increasing vesicularity (Fig. 5D) such that non-vesicular glass is mostly brown, whereas vesicular glass is mostly clear. Overall, the componentry thus shifts from ~50% felsite, 25% clear vesicular glass, and 25% poorly vesicular brown glass to 10% felsite, 10% clear glass, and 80% brown glass. Each observed texture (color and range of vesicularity) is present within almost every time sample.

Texture

Three-dimensional reconstruction of glass and felsite particles highlights textures and ferromagnesian crystal populations. The ferromagnesian crystal assemblage (pigeonite, augite, and titanomagnetite) is identical for felsite, clear glass, and brown glass and is the highest in crystalline felsite (8.2 vol%) and greater in clear glass than in brown glass (3 vol% and 0.4 vol%, respectively). These crystal phases are distributed as aggregates in felsite and as single crystals with embayments in the brown glass. Clear glass contains both single crystals and crystal aggregates (Supplementary material S5; see footnote 1). Previous petrographic analyses of the aggregates also found quartz and alkali feldspar with embayment texture when included in clear glass (Elders et al., 2011; Zierenberg et al., 2013). Vesicles with regular convex and/or concave shapes (as in Kennedy et al., 2016; Rhodes et al., 2018; Fig. 4A) are present in all particle types (glassy felsite, clear glass, and brown glass).

Size distributions of vesicle volume fraction for glassy felsite, clear glass, and brown glass, before and after the componentry change at ~17:15, are shown in Figure 6. The size distributions within single particles (Supplementary vesicle size distribution spreadsheet; see footnote 1) were sorted by glass color and time range and summed to obtain more statistically relevant vesicle size distributions (three glassy felsite, six clear glass, and three brown glass particles before 17:15; four clear glass and nine brown glass particles after 17:15). The characterization of the profile shape uses the approach of Shea et al. (2010). The overall distribution of shapes diverges for different retrieval times. Vesicles in clear glass retrieved early show a strongly normal distribution centered at 7.4 µm (17.5% volume). In brown glass, the distribution is centered at 4.7 µm (10.5% volume) but widely distributed and contains additional peaks. Both glass types contain a smaller peak at larger vesicle sizes (~59–75 µm). Glassy felsite has a similar vesicle population as the clear glass centered at 7.4 µm but has a significant secondary peak at ~29–38 µm.

After 17:15, the glass vesicle size distributions flatten similarly for the clear and brown glass (the maximum volume fractions decrease

Downloaded from http://pubs.geoscienceworld.org/gsa/gsabulletin/article-pdf/doi/10.1130/B35598.1/5211391/b35598.pdf
by Univ of California Davis Serials Dept, Robert A. Zierenberg

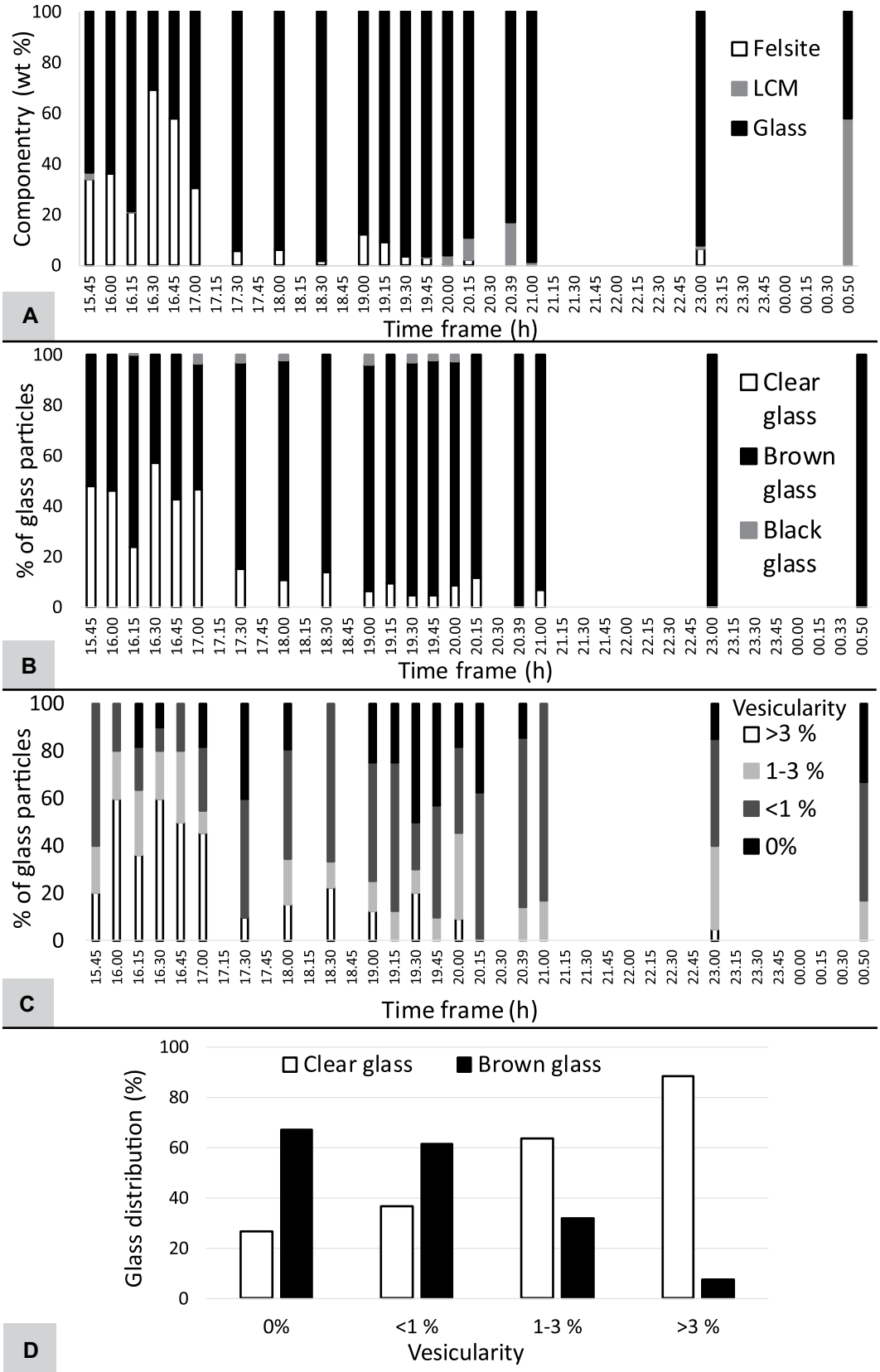

Figure 5. Componentry and textural variations in Iceland Deep Drilling Project-1 particles are shown. Time frames represent the absolute time of retrieval on 24 June 2009. (A) Componentry evolution of glass, felsite, and drilling contaminants (LCM—lost circulation material) over time of retrieval. (B) Evolution of glass color over time of retrieval in % of glass particles. As the contribution from black glass is minor, this type of glass is not considered further. (C) Variations of glass vesicularity over time of retrieval. (D) Relationship between glass color and vesicularity is shown, illustrating the similarities in variations of particles over time in panels B and C.

Downloaded from http://pubs.geoscienceworld.org/gsa/gsabulletin/article-pdf/doi/10.1130/B35598.1/5211391/b35598.pdf
by Univ of California Davis Serials Dept, Robert A. Zierenberg

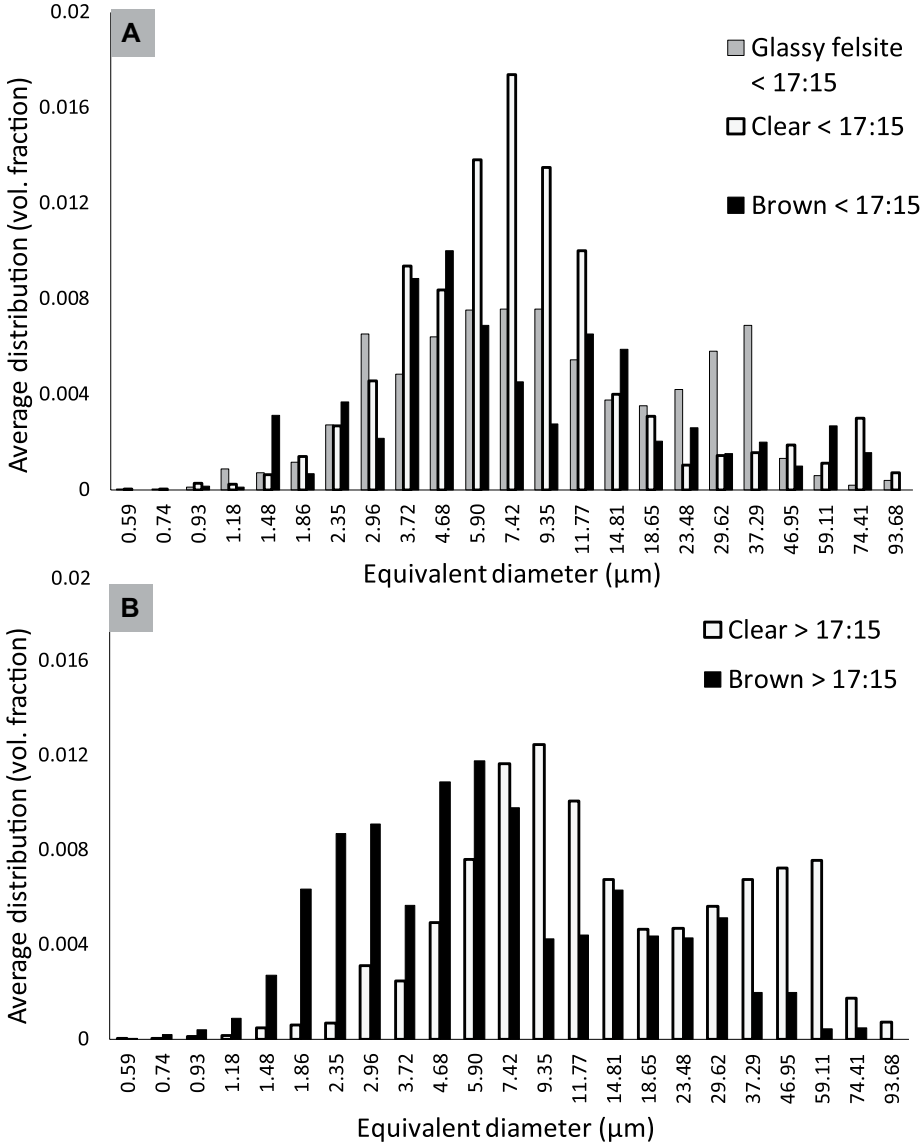

Figure 6. Vesicle volume fraction size distribution of glassy felsite, brown, and clear glass is shown (A) before and (B) after the componentry transition around 17:15. The distributions are averaged to avoid any bias from the number of particles analyzed.

to ~12%). But clear glass shows a higher abundance of larger vesicles (~37–59 μm), similar to the shape of the vesicle size distribution for early-retrieved glassy felsite, with larger vesicle sizes in the second peak than that of the glassy felsite (~23–37 μm). Conversely, brown glass particles show a higher proportion of small vesicles in addition to the larger vesicles. Irregularities in the vesicle size distribution of brown glass are unlikely to be artifacts given the large number of vesicles analyzed (n = 1760) and their presence in single particles as well as the summed size distribution shown in Figure 6 (see Supplementary vesicle size distribution spreadsheet).

Among the shape parameters analyzed, we observe a trend in the aspect ratio of vesicles. In the clear glass retrieved early, vesicle aspect ratios are in average per particle in the range of 0.35–0.61. This range shifts to 0.26–0.35 after 17:15. Similarly in brown glass, the average aspect ratio shifts from 0.61 to 0.66 to 0.30–0.54 (Supplementary vesicle size distribution spreadsheet). This variation is systematic despite the strong divergence of aspect ratio that can occur in a single glass particle (standard deviations are in the range 0.12–0.25; Fig. S4B). The aspect ratio of vesicles thus decreases over time of retrieval and shifts to more elongated shapes.

Major Elements

Compatible major element oxides (FeO, MgO, CaO) are plotted against SiO_2 (Fig. 7; Supplementary chemistry spreadsheet; see footnote 1). Clear glass tends to be higher in SiO_2, and brown glass tends to be higher in CaO, FeO, and MgO. Clear and brown glass define two clustered compositional end members, although some particles fall between these clusters (especially in MgO; Fig. 7A). The bulk felsite composition plots on the same trend. Our data partially overlap with the data from previous studies of IDDP-1 glass predominantly retrieved at 17:00, although the data sets have been classified slightly differently (Figs. 7B–7C). Zierenberg et al. (2013) divided the glass compositions into "Melt 1" (main glass component), "Melt 2" (interstitial glass within felsite), and "Melt 3" (crystal-rich glass). In contrast, Masotta et al. (2018) distinguished between rhyolite glass (which they termed "RHL") and interstitial glass in felsite composed of two end-members representing >70% and <8% partial melting of felsite (which they termed "FLS1" and "FLS2," respectively). Our classification is based on the dominant physical macro property of glass color. The three respective main glass components (Melt 1, RHL, and brown glass) consistently overlap. The dominant clear glass cluster is in close proximity to Melt 3 and a sub-group of FLS2 (Figs. 7B–7C). Two smaller clear glass clusters fall within the main glass component cluster or are adjacent to it and FLS1. Whether the wide range of compositions exhibited by the clear glass represents its true variability or is caused by subjective color misclassification is unclear; however, we consider the largest clear glass cluster to be representative of clear glass composition. Melt 2 (Zierenberg et al., 2013) and a sub-group of FLS2 (Masotta et al., 2018) overlap, but since we did not target the interstitial melt within the felsite in this study, none of our samples overlap these categories.

Glass Water Content and Its Isotopic Values

The TGA heating experiments show predominant mass loss from 600 °C to 1000 °C (Fig. S3). This result indicates insignificant low-temperature hydration (c.f. Denton et al., 2009; Giachetti et al., 2015) and thus dissolution of the water into the magma by a high-temperature process. The dTGA peaks (highest rates of mass loss) occur at 737 °C and 863 °C, matching the H_2O signal as determined by the mass spectrometer (Fig. S3), and confirming that dissolved $H_2O >> CO_2$ concentrations. Total water contents and hydrogen isotope ratios for clear and brown glass show no systematic variation with vesicularity or retrieval

Downloaded from http://pubs.geoscienceworld.org/gsa/gsabulletin/article-pdf/doi/10.1130/B35598.1/5211391/b35598.pdf
by Univ of California Davis Serials Dept, Robert A. Zierenberg

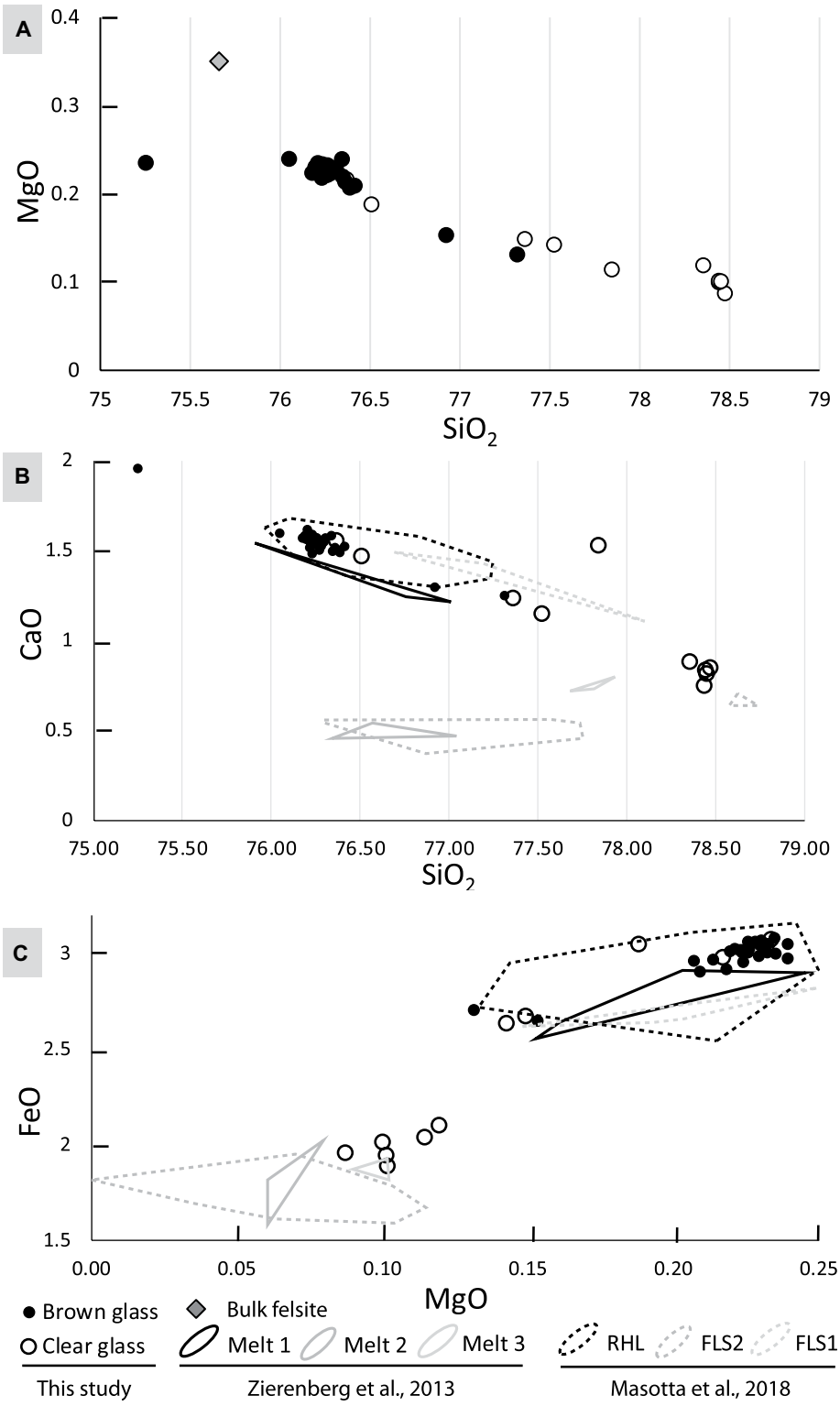

Figure 7. Major element chemistry (anhydrous) is shown for brown glass and clear glass. (A) MgO versus SiO_2; bulk felsite from Zierenberg et al. (2013). (B) CaO versus SiO_2. Comparison with data from Zierenberg et al. (2013; Melt 1, 2, and 3) and Masotta et al. (2018; RHL, FLS1, and FLS2). Melt 1 is described as the main glass component. Melt 2 is interstitial glass within felsite, and Melt 3 corresponds to crystal-rich glass and is interpreted as mixing of Melts 1 and 2. In Masotta et al. (2018), RHL is the main glass component and FLS1 and FLS2 are compositional end-members of interstitial glass in felsite, which fit with experimental results of felsite partial melting at high and low degrees, respectively. (C) FeO versus MgO compared to published data. We use convex hulls to enclose the clusters of previously published data points.

time (Supplementary water spreadsheet; see footnote 1). Water contents fall between 1.3 wt% and 2 wt%; the interquartile range is 1.64–1.92 wt% H_2O (Fig. 8A). δD values span a wide range from −120 wt% to −80‰, and the interquartile range is −115 wt% to −100‰ (Fig. 8A). Note that we cannot directly compare the range of major element compositions of particles with their water concentrations, as different particles were used for EPMA and TCEA analyses. Clear and brown glasses have slight but insignificant differences in H_2O (averages of 1.73 wt% and 1.81 wt%, respectively) and δD (–110 wt% and −107‰, respectively). Analysis of variance statistics were used to test the null hypothesis that the two glass types are the same on the basis of their water and deuterium compositions. Resulting low p-values of 0.1 and 0.3 indicate that the apparent groupings are not statistically different. The water and isotopic data are scattered but show a decrease in δD with water content (Fig. 8B). The particles plot between the trends defined by closed-system volcanic degassing (Newman et al., 1988) and secondary hydration (i.e., meteoric water added to the magma after its formation or to the glass; Seligman et al., 2016) on which Krafla epidotes also plot (Fig. 8B). However, we note that the secondary hydration trend relates to hydration of already-quenched pristine glasses, whereas there is no evidence, from water speciation and TGA experiments, for post-quenching hydration of particles. Instead, both $\delta^{18}O$ and δD values fall between those of unaltered mid-oceanic-ridge basalt (MORB) magma and hydrothermally altered phases. $\delta^{18}O$ values in IDDP-1 glass are higher than in Krafla epidotes (Elders et al., 2011), whereas our data show on average ~10‰ higher δD than epidotes and ~40‰ lower δD than the unaltered mantle (MORB averages at −60‰ δD, Fig. 8C).

DISCUSSION

Our interpretations are based on the assumption that the particles were retrieved in the same order as they were drilled (in spite of the dynamic downhole environment, the drilling stoppages, and drilling fluid interacting with hot magma) and therefore that they represent the sequence of lithologies/magma at depth. Particles of various

Downloaded from http://pubs.geoscienceworld.org/gsa/gsabulletin/article-pdf/doi/10.1130/B35598.1/5211391/b35598.pdf
by Univ of California Davis Serials Dept, Robert A. Zierenberg

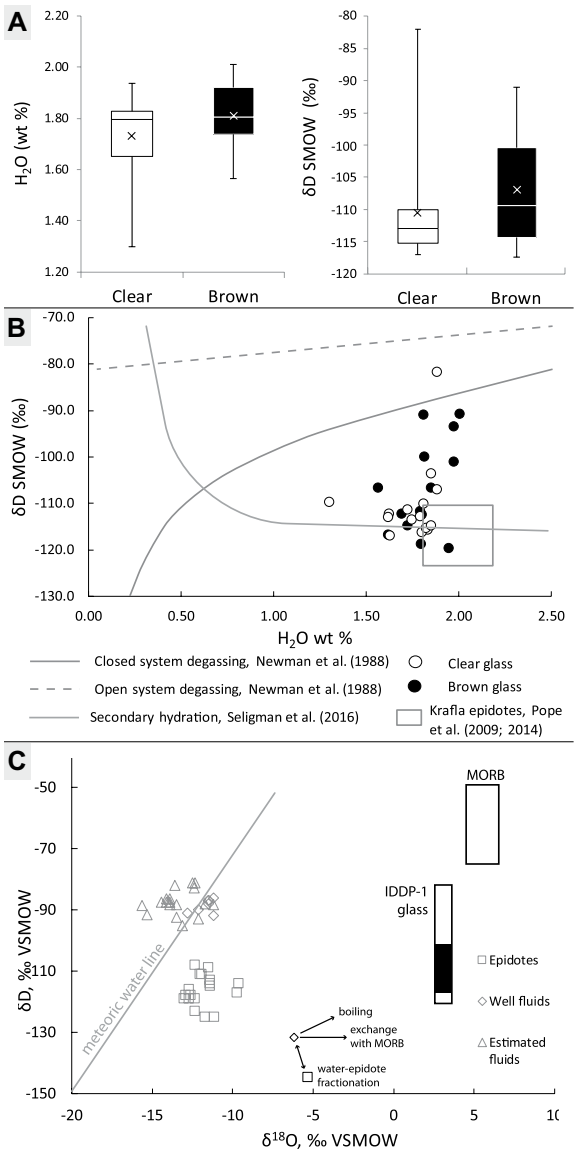

Figure 8. Water content and hydrogen and oxygen isotope systematics in Iceland Deep Drilling Project-1 glass particles compared to different styles of degassing, hydration, and known reservoir compositions. Analytical errors are ± 2‰ δD and ± 0.03 wt% H_2O. (A) Box plots of H_2O and δD for clear glass and brown glass (label in B: black = brown). Results show no relationship to vesicularity (Supplementary material; see footnote 1). (B) δD as a function of H_2O. The degassing trends are the minimum values for rhyolite with starting conditions estimated at 4 wt% H_2O and 0.1 wt% CO_2 at 500 bar (Newman et al., 1988); the secondary hydration line for quenched glass corresponds to the trend for high-latitude samples with low δD meteoric water values down to −120‰ (Seligman et al., 2016, 2018). The initial unaltered rocks are represented by the mid-oceanic-ridge basalt (MORB) composition (values from Clog et al., 2013). (C) Relationship between hydrogen and oxygen isotopes adapted from Zakharov et al. (2019). Krafla data epidotes, well fluid, and estimated fluid composition are from Pope (2011). δD range values in IDDP-1 glass data (the dark section represents the interquartile range) are combined with the $\delta^{18}O$ range from Elders et al. (2011). SMOW—standard mean ocean water; VSMOW—Vienna standard mean ocean water; MORB—mid-oceanic-ridge basalt.

types were retrieved concurrently at any given time, suggesting that some mixing of particles occurred (particles falling from the borehole walls and/or dynamic mixing caused by fluid circulation). However, our assumption is supported by the gradual change in componentry over time starting with felsite host rock (Fig. 5A). Evidence has already been presented for the host rock being felsite (geophysical data logs, shallower lithologies; Mortensen et al., 2014) and the magma being located at the bottom of the well (resulting in drilling difficulties; ISOR Iceland Geosurvey, 2009; Friðleifsson et al., 2010). Thus, we hold that the deepest particle samples were the last to be retrieved.

Scenarios for Magma Genesis and Reaction to Drilling

The results of this study are consistent with the presence of magma that is bimodal in composition and texture. Both clear glass and felsite were flushed out of the well earlier than the brown glass. The clear glass has higher crystal and SiO_2 content and higher vesicularity than the brown glass, and vesicle size distributions for the early retrieved particles (before 17:15) indicate a single dominant stage of nucleation and vesicle growth (Shea et al., 2010). The brown glass comprises the majority of the particles, and more widely distributed vesicle populations are interpreted to indicate punctuated vesicle nucleation. This brown glass is crystal-poor with higher FeO and MgO content.

The bimodal magma composition and texture can reflect genesis from two sources or differentiation from one source through fractional crystallization, fractional melting, or hydrothermal interactions. Previous geochemical data on IDDP-1 rhyolite glass support magma formation by partial melting of a felsite body that itself was derived from partial melting of hydrothermally altered basalt (Elders et al., 2011; Masotta et al., 2018). This interpretation fits with our glass composition categories and forms the starting point for refining (1) how the magma was generated and (2) how it reacted to drilling.

Key observations and interpretations are summarized in Table 1, where we collate and critically appraise evidence for alternative scenarios (genesis from two sources or differentiation from one source) and the impact of drilling on magma. Drilling may have affected the retrieved glass by triggering decompression-induced degassing, imparting stress that caused deformation, causing hydration that affected volatile chemistry, and/or sorting particles into a componentry that does not reflect the initial distribution. In the following sections, we present evidence for the partial melting scenario and accordingly explore the structure of the magma body and the timescale of the processes, which leads to a schematic representation of the possible architecture and origin of the IDDP-1 magma body (Fig. 9).

Structure and Generation of Rhyolite Magma

The four main observations about the major element compositions, including comparison with previously published data sets (Fig. 7; Zierenberg et al., 2013; Masotta et al., 2018), are: (1) the transition between the compositional end-members is gradational with only a limited overlap; (2) bulk felsite plots on the trendline of the glass toward the end of the brown glass range; (3) the composition of a large sub-group of clear glass plots toward a composition that is consistent with genesis from a small degree of felsite partial melting (near FLS2 generated by 8% felsite partial melting, Masotta et al., 2018; near Melt 3, glass containing crystals from felsite assimilation, Zierenberg et al., 2013); and (4) the composition of the brown glass plots on the trendline from the main melt (Melt 1 and RHL) toward higher degrees of felsite partial melting (>70% felsite partial melting that generated FLS1, Masotta et al., 2018). In addition, the interstitial glass within the felsite (Melt 2 of Zierenberg et al., 2013) is consistent with a very low

Downloaded from http://pubs.geoscienceworld.org/gsa/gsabulletin/article-pdf/doi/10.1130/B35598.1/5211391/b35598.pdf
by Univ of California Davis Serials Dept, Robert A. Zierenberg

TABLE 1. KEY OBSERVATIONS AND INTERPRETATIONS

Observation	Interpretation	Constraints on scenarios
Componentry		
Clear glass retrieved simultaneously with felsite	Close spatial relationship between clear melt and felsite	
Brown glass retrieved later	Located at greater depth	
Crystals		
Higher ferromagnesian crystallinity in clear glass, spatial distribution similar to that in felsite	Close spatial relationship between clear melt and felsite, favors assimilation or melting	
Texture of remelting in crystals	The melt is not crystallizing	No fractional crystallization
Vesicles		
Higher vesicularity in clear glass	Clear glass experienced more degassing than brown	
Larger vesicles in clear glass as time progresses	Clear glass experienced more coalescence associated with magma ascent	Drilling-induced magma movement
Smaller vesicles in brown glass as time progresses	Brown glass experienced more nucleation triggered by decompression with higher initial water content	Drilling-induced decompression
Initial normal size distribution in clear glass	Homogenous melt, homogenous reaction to drilling, not interstitial melt	Only limited sorting of particles through drilling
Secondary peaks in size distribution in brown glass	Punctuated nucleation or heterogenous melt	
Decrease in aspect ratio of vesicles over time	Deformation of vesicles while magma is intruding the well	Drilling-induced deformation
Texture of vesicle collapse in >3% vesicularity glass	Melts were vesicular and outgassing before magma rising	
Chemistry		
Progressive compositional transition in between the end-members	Gradation of degree of partial melting between two end-members	
Bulk felsite plots on the trendline of clear and brown glass	Felsite, clear, and brown melts are cogenetic	One common magma source
Brown glass chemistry is similar to high degree partial melting, conversely for clear glass	Brown melt represents almost complete partial melting of felsite.Clear melt formed by low degree of partial melting	
Volatiles		
From TGA, no second hydration peak in glass, mass loss >600°C	No sub-Tg hydration by meteoric or drilling fluids, hydration at high temperature	No alteration/hydration by drilling fluids
Large range of δD values, plotting between MORB and epidotes	Mixing of magmatic water with hydrothermal water	Felsite hydration from both deeper magma and hydrothermal fluids

Note: TGA—thermogravimetric; MORB—mid-oceanic-ridge basalt.

degree of partial melting (<8%, as evidenced by its overlap with a subgroup of FLS2) and does not occur as single particles.

Observation (1) supports the assertion that clear and brown glass were either derived from magmas that were cogenetic, with the compositional transition reflecting gradual variation of partial melting or crystallization, or else derived from variable mixing between two magmas. The fact that there are embayed crystals in both the brown glass and the clear glass, however, indicates partial melting of the crystals (resorption) or crystal transfer and disequilibrium associated with magma mixing (Fig. 4D; Masotta et al., 2018). Observation (2) supports a cogenetic origin of felsite and both types of glass. Therefore, the two magmas can be seen as subsets of one magma reservoir generated and evolving in a similar manner. The majority of our analyses and those presented previously (Masotta et al., 2018; Zierenberg et al., 2013) cluster into compositional groups consistent with differences in the sample's glass color. However, there are a few glass particles with intermediate compositions that represent variable degrees of partial melting. It is possible that despite our efforts to standardize color definitions, subjectivity may have played a role in the visual classification of these intermediate glass particles as either clear or brown. Overall, accounting for all four observations, our results suggest that the degree of partial melting was generally bimodal. The low proportion of single glass particles plotting between the two clear and brown glass end-

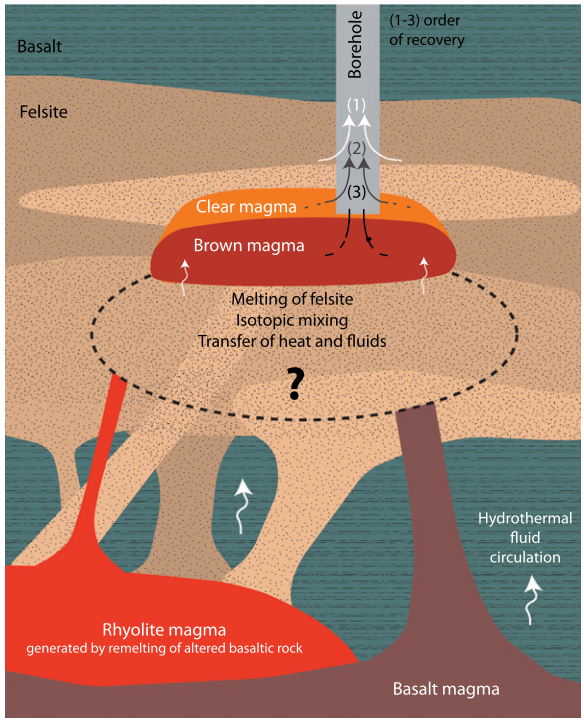

Figure 9. Schematic of Iceland Deep Drilling Project-1 rhyolite magma body and well are shown but not to scale. The true reservoir shape is not constrained. Heat and hydration from the main basalt magma chamber at 4 km depth can locally trigger rhyolite genesis at the margins through partial melting of hydrothermally altered basalt bodies. This rhyolite magma can then form a network of silicic intrusions and become cogenetic host felsite when crystallizing (see dotted felsite bodies). Intrusion of rhyolitic or basaltic magma into the felsite provides heat and magmatic fluids, which can flux into the felsite and promote partial melting of this host rock. This is possibly aided by circulation of hot hydrothermal fluids. The brown, crystal-poor rhyolite magma is generated by a high degree of felsite melting, and a lower degree of melting at the margins forms the clear, vesicular rhyolite magma that is SiO_2^- and crystal-rich. Partial melting of felsite prevents the formation of a chilled margin, and the spatial distribution of the clear and brown magmas indicates that homogenizing magma convection is insignificant in the remelted body. Well intersection allowed recovery of host felsite, clear glass, and finally the brown glass (order of retrieval 1–3 is indicated). Decompression and deformation of the magma prior to quenching by drilling fluids triggered additional coalescence and nucleation of vesicles. Low-degree melting of the felsite is ongoing.

Downloaded from http://pubs.geoscienceworld.org/gsa/gsabulletin/article-pdf/doi/10.1130/B35598.1/5211391/b35598.pdf
by Univ of California Davis Serials Dept, Robert A. Zierenberg

members, the limited mixing textures (we found no mingled particles like those described in Zierenberg et al., 2013), and the textural overlap between crystal aggregates in the clear glass and the crystalline felsite suggest that partial melting occurred in situ.

The distinction in vesicle size distribution between clear and brown glass (Fig. 6) and the presence of a modest chemical continuum between two end-members (Fig. 7) suggests the two end-member magmas resided as discrete, adjacent layers that were most likely related to a spatial gradient in the degree of partial melting. If the interpretation of discrete storage of magmas is correct, then magma convection (Eichelberger, 2019) was not sufficient to mix or significantly mingle these magmas.

Componentry also allows us to explore whether the drill directly intersected a pocket of magma or instead intersected a magma distributed within crystal mush interstices (Eichelberger et al., 2017; c.f. Holness, 2018). Particles with the interstitial glass composition (such as those in Melt 2; Zierenberg et al., 2013) are absent from the single glass particles studied here and are therefore likely rare. This observation does not support an efficient draw-out of magmas through interstices between crystals in felsite. We therefore propose that the drill either reached a magma pocket or was extremely close to a magma body connected to the borehole by a fracture network.

The felsite and clear glass particles have similar crystal aggregates, with embayed crystals in clear glass suggesting felsite partial melting (Fig. 4D, Material S5). The clear glass generally has higher crystal content than the brown glass (Material S5), which also supports a close spatial and genetic relationship between clear magma and felsite. The componentry is additional evidence for this clear magma/felsite relationship: the transition around 17:15 (Fig. 5) suggests a shift from (1) retrieval of similar quantities of glass and host felsite, with near equal contribution of clear and brown glass, to (2) retrieval dominated by poorly vesicular brown glass with minor and similar contributions of felsite and clear glass. We interpret that the magma from which the clear glass is derived is stored at shallower levels than the brown glass and could have formed the top of the rhyolitic magma body. Thus, the shift in componentry could relate to the disruption of the partially melted roof of the magma body (Fig. 9).

A complication arises when reconciling the water content of the rhyolite glass with rhyolite magma formation through partial melting of felsite. Melting of the largely anhydrous felsite (0.23 wt% LOI; Zierenberg et al., 2013) would not generate a magma with the water content as high as that measured in either the clear or brown rhyolitic glass (1.77 wt%). The water in the rhyolite glasses must therefore have been added by another process. The TGA dehydration experiment shows no peaks associated with secondary hydration by meteoric water, and the measured patterns of volatile release indicate high-temperature diffusive loss of water (Denton et al., 2009; Giachetti et al., 2015; Fig. S2). Furthermore, high OH/H_2O_m ratios do not support secondary hydration (Zierenberg et al., 2013; Watson, 2018). Together, these results refute the hypothesis that there was any significant post quenching addition of drilling fluids (water) into the glass, which would nonetheless be difficult to reconcile with the slow rate of water diffusion in rhyolite glass ($\sim$9–12 $\times$ 10^{-8} cm^2/s at 900 °C; Doremus, 1995). Instead, it supports that any uptake of water must have occurred at high temperatures (>Tg) perhaps during the partial melting process.

The δD and $\delta^{18}O$ data are examined to constrain the origin of this hydration. Variations in the δD value among the IDDP-1 glass particles could be explained by variations in the source rock, by volatile fractionation during magma degassing, or by mixing between two sources. In Iceland, variation in the hydrothermally altered basalt source rock of the felsite could relate to the broad range of δD, covering epidotes and well fluids, and their slight decrease with decreasing water content ($\sim$–30‰ for $\sim$–0.4 wt% H_2O, Figs. 8B–8C). But in such a case, we might expect a stronger correlation between major element chemistry, water content, and δD in the rhyolitic glasses as well as a higher water content of the host felsite. A volatile fractionation alternative would be restricted to an early stage in the degassing history: high δD water could be lost during fractionation, and thus the higher δD endmember would be closer to the initial isotopic signature, which plots on the degassing trend (Fig. 8B). However, the degassing gradient in the IDDP-1 data is steeper than that of mantle-derived rhyolite from Newman et al. (1988). Also, exsolving significant volumes of high δD water into vesicles is unlikely, as the glass particles do not contain many vesicles. Instead, mixing of water from two sources might best explain the isotopic composition. Both the δD and $\delta^{18}O$ data from the clear glass and brown glass indicate an isotopic signature intermediate between magmatic water from MORB and meteoric hydrothermal fluids (Fig. 8C). This requires an initial input of magmatic water from a main, deep, basalt magma chamber and also an input of meteoric water from the hydrothermal system. Considering the low water content of felsite in direct contact with the rhyolite magma, hydration is unlikely to have occurred prior to the melting process. Hot hydrothermal fluids (mixed meteoric and magmatic) could potentially be fluxed and incorporated during felsite partial melting, although more work is required to test this hypothesis. Alternatively, another hot magma could be the source of heat and fluids, in which case transfer of water from this saturated magma to the under-saturated rhyolite magma might have occurred.

The exact magmatic configuration of the IDDP-1 rhyolite magma body is not fully constrained by the geochemical and textural results presented here nor the work of other authors. However, we demonstrate the occurrence of in situ felsite partial melting at the bottom of the well and the coexistence of two magmas that correspond to two main degrees of partial melting. The felsite makes up most of the lithology below 2020 mbs and thus a thickness of $\sim$80 m above the intersected rhyolitic magma (Mortensen et al., 2014). The most plausible source of the fluids and heat required to remelt the felsite is adjacent fresh magma. However, this hypothetical magma has not been sampled and could be composed of basalt or hot rhyolite. Hydration from fluxed, high-temperature hydrothermal fluids could have also played a role in the remelting of felsite. The processes involved in the IDDP-1 rhyolite magma genesis, through partial melting of felsite above an unconstrained heat and fluid source, are illustrated in Figure 9.

Timescale of Degassing

We explore the degassing signatures in the glass using vesicle textures in relation to the timeline of drilling events (Fig. S1). The vesicle size distributions in the glass represent the vesicle populations in the magma at the time of quenching. We assume that quenching induced by drilling fluids was rapid enough to prevent significant water resorption and bubble shrinkage (McIntosh et al., 2014) as well as secondary hydration. The normal profile distribution in early-retrieved clear glass supports a single degassing event (Fig. 6; Shea et al., 2010) of what we interpret to be a homogenous magma. In brown glass, peaks are interpreted to indicate punctuated nucleation (Fig. 6; Shea et al., 2010). The appearance of a new small vesicle population in brown glass after 17:15 suggests that nucleation was triggered by a step of drilling-induced decompression, which occurred after the nucleation and volatile resorption/outgassing of the main vesicle populations within this magma (Fig. 6). In clear glass, the distribution shows an increase in large vesicles after 17:15, indicating secondary growth processes that we propose were mostly coalescence based on the distribution and the textural evidence in thin sections (Fig. 4B; Shea et al., 2010).

Downloaded from http://pubs.geoscienceworld.org/gsa/gsabulletin/article-pdf/doi/10.1130/B35598.1/5211391/b35598.pdf
by Univ of California Davis Serials Dept, Robert A. Zierenberg

Magma deformation associated with shear stress during magma movement can favor local coalescence even in poorly vesicular and viscous magmas (Okumura et al., 2006; Okumura et al., 2009; Caricchi et al., 2011). Retrieved particles show elongated vesicles, irregular vesicles, and vesicles frozen in mid-coalescence, which we interpret as evidence for shear and minor outgassing (Figs. 4A–4C, Fig. S4; Okumura et al., 2006; Kushnir et al., 2017). The systematic decrease in the aspect ratio of vesicles in particles retrieved after 17:15 (Supplementary vesicle size distribution spreadsheet; see footnote 1) means that the vesicles in the samples retrieved later are more elongated. The change was possibly due to deformation related to magma movement (e.g., Kushnir et al., 2017), which could have been induced by drilling, and is also in agreement with the occurrence of coalescence. We observe that the vesicle size distribution in early-retrieved glassy felsite is similar to that of the clear glass retrieved after 17:15 and shows a dominant single stage of nucleation and growth plus an abundance of larger sizes. This similarity suggests the glassy felsite reacted to drilling in a similar way as the clear magma but earlier in the time-series. Thus, it was located at a shallower depth: at the transition between crystalline felsite and clear magma.

We interpret that the changes in vesicle size distributions after 17:15 are dominantly drilling-related and affected both clear and brown glass, whereas distributions before 17:15 could be related to drilling-induced or older decompression events. One or both of the two previous magma intersections (50 days and 16 days before) are possibilities, or else these distributions could represent initial magmatic textural states. The nature of the single nucleation peak in clear glass indicates that it is unlikely that the magma decompression was related to the previous magma intersection events that occurred nearby.

Most of the vesicular glass has textural evidence indicative of vesicle collapse (Fig. 4A). However, it is unclear whether these vesicle populations are related to drilling or if they pre-existed in the undisturbed magma. The proposed timescales of progression from vesicle nucleation to collapse by outgassing or resorption in silicic magmas are on the order of hours (>5 h, Martel and Iacono-Marziano, 2015; 0.5–10 h, Kennedy et al., 2016; Yoshimura et al., 2019). Thus, it is possible that these processes occurred within the 45–60 min interval between magma intersection and magma rising into the well but not during the rise itself. Assuming the vesiculation observed from 17:15 relates to a rapid magma rise, the related bubble size distributions should thus have been unaffected by vesicle collapse.

The timescale of degassing is explored considering constraints on the spatial relationship between the magmas and their surroundings and depends on the magma viscosity. Here, using the glass compositions and water contents (Supplementary data spreadsheet; see footnote 1) and the silicate melt viscosity calculator of Giordano et al. (2008), we obtain viscosities of $10^{6.14}$ and $10^{5.95}$ Pa.s^{-1} at 900 °C for clear and brown magmas, respectively. This temperature, indicated by mineral thermo-barometry (Zierenberg et al., 2013), represents the most likely temperature at the time of magma intersection rather than quench temperatures (e.g., Watson, 2018). Crystals and vesicles are not included in the viscosity calculation and would modify the magma rheology, but their low proportion makes this effect negligible (e.g., Mader et al., 2013). As drilling caused quenching of magma, the timescale for vesicle growth, nucleation, coalescence, or outgassing decreases compared to that calculated from decompression only (Martel and Iacono-Marziano, 2015; Yoshimura et al., 2019). When the drill bit reached magma, drillers repeatedly pulled back and pushed down in attempts to keep the drill bit free. The time frame for the magma to react to drilling-induced decompression (Fig. S1) includes an interval of 45–60 min between the start of magma intersection by the third leg and its ascent into the well, among which there are nine minutes between the last drilling approach to the bottom of the well and first evidence of magma ascending up the well. There is also a ~4 min interval during which the magma rose 9 m up the well and a further maximum period of 3 h between magma ascent and the observation of vesicle coalescence in the glass. Independently from our conclusions about vesicle size distributions, these intervals could be sufficient to develop the full variety of vesicle textures observed in the clear and brown glass (e.g., Navon and Lyakhovsky, 1998).

The population of the smallest vesicles in the brown magma is interpreted to have been formed by nucleation triggered by the decompression associated with exposure to wellbore hydrostatic pressure and subsequent magma rise up the well, whereas other vesicle populations could have existed beforehand. To test this hypothesis, we first compare the matrix Bubble Number Density (matrix-BND, number of vesicle per unit of volume, Toramaru, 2014) corresponding to the smallest vesicle population in the brown magma (<3 μm in diameter for eight brown glass particles retrieved after 17:15) to the BND of larger vesicles in the same magma. The matrix-BND is in the range of 10^{14}–10^{15} m^{-3}, many orders of magnitude higher than the BND of the supposed pre-existing vesicles, which is 10^{4}–10^{5} m^{-3}. This value of matrix-BND is expected for cases of secondary nucleation (Toramaru, 2014). The matrix-BND can be used in the bubble rate meter for explosive eruptions and homogeneous nucleation developed by Toramaru (2006), resulting in a decompression rate for the brown magma in the range of 10^{6}–10^{7} Pa s^{-1}. The decompression felt by the magma at 2104 mbs can be estimated considering that the magma was first stored at lithostatic pressure (density of host volcanic rocks ~2500 kg/m^3) and then suddenly connected to the well at hydrostatic pressure. The pressure difference is 29 MPa. Over the 9 min between the last magma approach at the bottom of the well and the first evidence of rising magma, the decompression could have been slow and progressive or quick and delayed. If progressive, the average decompression rate would be 5.4×10^{4} Pa s^{-1}. This estimate is far lower than the rate calculated from the matrix-BND, which only fits a near-instantaneous decompression event. Standpipe pressure in the well, which cannot be directly applied to pressure at the base of the well, does indicate several sharp spikes and dips (Fig. S1). We conclude that the magma underwent one, or several, rapid decompression events associated with the puncturing of a low permeability layer at the interface, such as a plug of quenched magma. We consequently propose that most of the vesicularity in the intersected magmas existed prior to the magma reaction to drilling and was modified by some additional bubble nucleation in the brown magma and subsequent bubble growth and deformation in the clear magma during magma rise up the borehole.

Implications

Remelting of host rocks around shallow magma is important to consider for deep geothermal prospecting and volcanic hazard assessment; partially melted rhyolite may contribute to the volumes and heat budgets of shallow intrusive systems but can be difficult to detect from the surface. Importantly, the IDDP-1 rhyolite magma at Krafla does not appear to be crystallizing; crystals with partially melted surfaces suggest ongoing partial melting, and it is surrounded by felsite containing a high proportion of interstitial melt (glassy felsite). We conclude that the intersected rhyolite magma body is at the very least maintaining its volume and likely continuing to enlarge, with low degree partial melting of host felsite occurring at its margins. Its geothermal potential is therefore likely to continue to increase, and with its potential for rapid heat recharge (e.g., Axelsson et al., 2014), the IDDP-1 magma body could be exploited as a source of geothermal energy. The viability of future drilling will require that the poorly understood deep source of heat and fluids at the origin

Downloaded from http://pubs.geoscienceworld.org/gsa/gsabulletin/article-pdf/doi/10.1130/B35598.1/5211391/b35598.pdf
by Univ of California Davis Serials Dept, Robert A. Zierenberg

of the IDDP-1 magma body be better characterized. Furthermore, thorough understanding of partial melting of crystal-rich silicic lithologies and adequate geophysical detection of shallow silicic magma bodies are critical for monitoring restless calderas and exploring deep geothermal energy resources.

This study also provides insight into the behavior of subsurface rhyolite magma. The overlying relationship of the clear to the brown magma within the IDDP-1 rhyolite magma reservoir, and the scarcity of compositions between the clear and brown glass, support a bimodal partial melting model. The vesiculation of the magmas prior to rising, and textures of vesicle collapse, reveal saturated magma that is highly sensitive to pressure differences.

CONCLUSION

The development of plans to redrill the currently capped IDDP-1 well at Krafla and deliberately re-intersect the rhyolite magma at 2104 mbs (KMT project; Eichelberger, 2019) will benefit from this detailed study of particles retrieved at regular time intervals after magma intersection. Characterization of textures, compositions, and volatile species yield new constraints on the scenario of partial melting and provide insights into magma genesis, storage, and reaction to drilling, which is also crucial for mitigating hazards in the Krafla geothermal field.

In summary, the IDDP-1 magma body is an example of shallow rhyolite generated by partial melting of a cogenetic host felsite in an intrusive system. Our results support an origin of two distinct rhyolite magmas from felsite partial melting ultimately driven by deeper basalt magmatism and aided by hydration from both magmatic and hydrothermal fluids. The resulting magmas coexist as discrete layers with little evidence for mixing. Our textural and geochemical associations between the clear and brown glass particles and the host felsite particles support a model of a small volume of clear rhyolite magma generated in situ via small degree felsite partial melting at the top of a layer of brown rhyolite magma that is generated via a higher degree of felsite partial melting. The textures of the resorbed crystals, with no evidence of crystallization, indicates that melting of felsite is ongoing and hence that the magma volume could be increasing.

The drilling triggered a rapid decompression of the magmas (10^6–10^7 Pa s^{-1}), causing the clear magma to vesiculate further and some additional vesicles to nucleate in the brown magma. Magma decompression and movement up the well is highlighted by a major shift in componentry and vesicle texture after ~2 h of particle retrieval: the quantity of brown glass particles critically increased (~50% felsite, 25% clear vesicular glass, and 25% poorly vesicular brown glass shifted to 10% felsite, 10% clear glass, and 80% brown glass), and the vesicles became more elongated with a decrease in aspect ratio. The IDDP-1 rhyolite magma body is thus highly sensitive to pressure perturbations.

AUTHOR CONTRIBUTIONS

The study was led by E. Saubin under the supervision of B. Kennedy, M. Villeneuve, and H. Tuffen. The manuscript and figures were prepared by E. Saubin with contributions from all authors. Textural data were collected by E. Saubin and H. Tuffen, and analyses of major elements and volatile contents were performed by E. Saubin and T. Watson with C.I. Schipper. TCEA measurements of δD and H_2O were conducted by I. Bindeman, who also provided an unpublished data set. F.B. Wadsworth provided the CT scans that E. Saubin and C.I. Schipper used for 3-D motions. Statistics were calculated by E. Saubin. A. Mortensen, and R. Zierenberg, and M. Villeneuve brought knowledge in terms of drilling engineering and the petrology of the Krafla rhyolite. Interpretations were built by E. Saubin, who was helped by all of the authors.

ACKNOWLEDGMENTS

The authors thank the Iceland Deep Drilling Project and Landsvirkjun for providing the raw samples. This work was supported by the Ministry of Business, Employment and Innovation, New Zealand (grant number E6552) and a Royal Society University Research Fellowship to H. Tuffen. I. Bindeman thanks National Science Foundation grant EAR1822977 for support. INB acknowledges support from the Russian Science Foundation (grant RNF19-17-00241). The authors also thank two anonymous reviewers and Jocelyn McPhie from GSA Bulletin, John Eichelberger, and Cecile Massiot, who provided constructive feedback that helped to improve this manuscript.

REFERENCES CITED

Applegarth, L.J., Tuffen, H., James, M.R., and Pinkerton, H., 2013, Degassing-driven crystallisation in basalts: Earth-Science Reviews, v. 116, p. 1–16, https://doi.org/10.1016/j.earscirev.2012.10.007.

Ármannsson, H., Fridriksson, T., Gudfinnsson, G.H., Ólafsson, M., Óskarsson, F., and Thorbjörnsson, D., 2014, IDDP—The chemistry of the IDDP-01 well fluids in relation to the geochemistry of the Krafla geothermal system: Geothermics, v. 49, p. 66–75, https://doi.org/10.1016/j.geothermics.2013.08.005.

Axelsson, G., Egilson, T., and Gylfadóttir, S.S., 2014, Modelling of temperature conditions near the bottom of well IDDP-1 in Krafla, Northeast Iceland: Geothermics, v. 49, p. 49–57, https://doi.org/10.1016/j.geothermics.2013.05.003.

Björnsson, A., 1985, Dynamics of crustal rifting in NE Iceland: Journal of Geophysical Research: Solid Earth, v. 90, p. 10151–10162, https://doi.org/10.1029/JB090iB12p10151.

Bostick, N.H., and Pawlewicz, M.J., 1984, Paleotemperatures based on vitrinite reflectance of shales and limestones in igneous dike aureoles in the Upper Cretaceous Pierre Shale, Walsenburg, Colorado, *in* Woodward, J.G., Meissner, F.F., and Clayton, C.J., eds., Hydrocarbon Source Rocks of the Greater Rocky Mountain Region: Denver, Colorado, Rocky Mountain Association of Geologists, p. 387–392.

Brandsdóttir, B., Menke, W., Einarsson, P., White, R.S., and Staples, R.K., 1997, Färoe-Iceland Ridge Experiment 2. Crustal structure of the Krafla central volcano: Journal of Geophysical Research. Solid Earth, v. 102, p. 7867–7886, https://doi.org/10.1029/96JB03799.

Caricchi, L., Pommier, A., Pistone, M., Castro, J., Burgisser, A., and Perugini, D., 2011, Strain-induced magma degassing: Insights from simple-shear experiments on bubble bearing melts: Bulletin of Volcanology, v. 73, p. 1245–1257, https://doi.org/10.1007/s00445-011-0471-2.

Castro, J.M., Bindeman, I.N., Tuffen, H., and Ian Schipper, C., 2014, Explosive origin of silicic lava: Textural and δD-H2O evidence for pyroclastic degassing during rhyolite effusion: Earth and Planetary Science Letters, v. 405, p. 52–61, https://doi.org/10.1016/j.epsl.2014.08.012.

Clog, M., Aubaud, C., Cartigny, P., and Dosso, L., 2013, The hydrogen isotopic composition and water content of southern Pacific MORB: A reassessment of the D/H ratio of the depleted mantle reservoir: Earth and Planetary Science Letters, v. 381, p. 156–165, https://doi.org/10.1016/j.epsl.2013.08.043.

Denton, J.S., Tuffen, H., Gilbert, J.S., and Odling, N., 2009, The hydration and alteration of perlite and rhyolite: Journal of the Geological Society, v. 166, p. 895–904, https://doi.org/10.1144/0016-76492008-007.

Doremus, R.H., 1995, Diffusion of water in silica glass: Journal of Materials Research, v. 10, p. 2379–2389, https://doi.org/10.1557/JMR.1995.2379.

Eggertsson, G.H., 2019, Constraining mechanical and permeability properties of the Krafla geothermal reservoir, North-East Iceland [Ph.D. thesis]: Liverpool, England, University of Liverpool, 119 p.

Eichelberger, J., 2019, Magma: a journey to inner space: Eos Science News by AGU, v. 100, p. 26–31.

Eichelberger, J., Carrigan, C., Sun, Y., and Lavallee, Y., 2017, Why is there an abrupt transition from solid rock to low crystallinity magma in drilled magma bodies: Abstract NH11A–0097 presented at 2017 AGU Fall Meeting, New Orleans, Louisiana, 11–15 December.

Einarsson, P., 1978, S-wave shadows in the Krafla Caldera in NE-Iceland, evidence for a magma chamber in the crust: Bulletin Volcanologique, v. 41, no. 3, p. 187–195, https://doi.org/10.1007/BF02597222.

Elders, W.A., Friðleifsson, G.Ó., Zierenberg, R.A., Pope, E.C., Mortensen, A.K., Guðmundsson, Á., Lowenstern, J.B., Marks, N.E., Owens, L., Bird, D.K., Reed, M., Olsen, N.J., and Schiffman, P., 2011, Origin of a rhyolite that intruded a geothermal well while drilling at the Krafla volcano, Iceland: Geology, v. 39, p. 231–234, https://doi.org/10.1130/G31393.1.

Friðleifsson, G.Ó., Pálsson, B., Stefánsson, B., Albertsson, A., Gunnlaugsson, E., Ketilsson, J., Lamarche, R., and Andersen, P., 2010, Iceland Deep Drilling Project. The first IDDP drill hole drilled and completed in 2009, *in* Proceedings of the World Geothermal Congress, Bali, Indonesia, 25–29 April 2010.

Friðleifsson, G.Ó., Elders, W., and Bignall, G., 2013, A plan for a 5 km-deep borehole at Reykjanes, Iceland, into the root zone of a black smoker on land: Scientific Drilling, v. 16, p. 73–79, https://doi.org/10.5194/sd-16-73-2013.

Friðleifsson, G.Ó., Ármannsson, H., Guðmundsson, Á., Árnason, K., Mortensen, A.K., Pálsson, B., and Einarsson, G.M., 2014, Site selection for the well IDDP-1 at Krafla: Geothermics, v. 49, p. 9–15, https://doi.org/10.1016/j.geothermics.2013.06.001.

Giachetti, T., Gonnermann, H.M., Gardner, J.E., Shea, T., and Gouldstone, A., 2015, Discriminating secondary from magmatic water in rhyolitic matrix-glass of volcanic pyroclasts using thermogravimetric analysis: Geochimica et Cosmochimica Acta, v. 148, p. 457–476, https://doi.org/10.1016/j.gca.2014.10.017.

Giordano, D., Russell, J.K., and Dingwell, D.B., 2008, Viscosity of magmatic liquids: A model: Earth and Planetary Science Letters, v. 271, no. 1, p. 123–134, https://doi.org/10.1016/j.epsl.2008.03.038.

Downloaded from http://pubs.geoscienceworld.org/gsa/gsabulletin/article-pdf/doi/10.1130/B35598.1/5211391/b35598.pdf
by Univ of California Davis Serials Dept, Robert A. Zierenberg

Hamada, M., Laporte, D., Cluzel, N., Koga, K.T., and Kawamoto, T., 2010, Simulating bubble number density of rhyolitic pumices from Plinian eruptions: Constraints from fast decompression experiments: Bulletin of Volcanology, v. 72, p. 735–746, https://doi.org/10.1007/s00445-010-0353-z.

Holness, M.B., 2018, Melt segregation from silicic crystal mushes: A critical appraisal of possible mechanisms and their microstructural record: Contributions to Mineralogy and Petrology, v. 173, p. 48, https://doi.org/10.1007/s00410-018-1465-2.

Hudak, M., and Bindeman, I.N., 2018, Conditions of pinnacle formation and glass hydration in cooling ignimbrite sheets from H and O isotope systematics at Crater Lake and the Valley of Ten Thousand Smokes: Earth and Planetary Science Letters, v. 500, p. 56–66, https://doi.org/10.1016/j.epsl.2018.07.032.

Ingason, K., Kristjánsson, V., and Einarsson, K., 2014, Design and development of the discharge system of IDDP-1: Geothermics, v. 49, p. 58–65, https://doi.org/10.1016/j.geothermics.2013.05.002.

ISOR Iceland Geosurvey, 2009, IDDP-1—Krafla, Vitismor—Production casing, drilling report no. 119.

Jarosewich, E., Nelen, J.A., and Norberg, J.A., 1980, Reference samples for electron microprobe analysis: Geostandards Newsletter, v. 4, no. 1, p. 43–47, https://doi.org/10.1111/j.1751-908X.1980.tb00273.x.

Jochum, K.P., Nohl, U., Herwig, K., Lammel, E., Stoll, B., and Hofmann, A.W., 2005, GeoReM: A new geochemical database for reference materials and isotopic standards: Geostandards and Geoanalytical Research, v. 29, p. 333–338, https://doi.org/10.1111/j.1751-908X.2005.tb00904.x.

Jónasson, K., 1994, Rhyolite volcanism in the Krafla central volcano, north-east Iceland: Bulletin of Volcanology, v. 56, p. 516–528, https://doi.org/10.1007/BF00302832.

Kennedy, B.M., Wadsworth, F.B., Vasseur, J., Schipper, C.I., Jellinek, A.M., von Aulock, F.W., Hess, K., Russell, J.K., Lavallée, Y., Nichols, A.R.L., and Dingwell, D.B., 2016, Surface tension driven processes densify and retain permeability in magma and lava: Earth and Planetary Science Letters, v. 433, p. 116–124, https://doi.org/10.1016/j.epsl.2015.10.031.

Kennedy, B.M., Holohan, E.P., Stix, J., Gravley, D.M., Davidson, J.R.J., and Cole, J.W., 2018, Magma plumbing beneath collapse caldera volcanic systems: Earth-Science Reviews, v. 177, p. 404–424, https://doi.org/10.1016/j.earscirev.2017.12.002.

Kushnir, A.R., Martel, C., Champallier, R., and Arbaret, L., 2017, In situ confirmation of permeability development in shearing bubble-bearing melts and implications for volcanic outgassing: Earth and Planetary Science Letters, v. 458, p. 315–326, https://doi.org/10.1016/j.epsl.2016.10.053.

Limaye, A., 2012, Drishti: A volume exploration and presentation tool, *in* Proceedings, SPIE 8506, Developments in X-Ray Tomography VIII, 85060X, https://doi.org/10.1117/12.935640.

Mader, H.M., Llewellin, E.W., and Mueller, S.P., 2013, The rheology of two-phase magmas: A review and analysis: Journal of Volcanology and Geothermal Research, v. 257, p. 135–158, https://doi.org/10.1016/j.jvolgeores.2013.02.014.

Marsh, B.D., Gunnarsson, B., Congdon, R., and Carmody, R., 1991, Hawaiian basalt and Icelandic rhyolite: Indicators of differentiation and partial melting: Geologische Rundschau, v. 80, p. 481–510, https://doi.org/10.1007/BF01829378.

Martel, C., and Iacono-Marziano, G., 2015, Timescales of bubble coalescence, outgassing, and foam collapse in decompressed rhyolitic melts: Earth and Planetary Science Letters, v. 412, p. 173–185, https://doi.org/10.1016/j.epsl.2014.12.010.

Martin, E., Bindeman, I.N., Balan, E., Palandri, J., Seligman, A., and Villemant, B., 2017, Hydrogen isotope determination by TC/EA technique in application to volcanic glass as a window into secondary hydration: Journal of Volcanology and Geothermal Research, v. 348, p. 49–61, https://doi.org/10.1016/j.jvolgeores.2017.10.013.

Masotta, M., Mollo, S., Nazzari, M., Tecchiato, V., Scarlato, P., Papale, P., and Bachmann, O., 2018, Crystallization and partial melting of rhyolite and felsite rocks at Krafla volcano: A comparative approach based on mineral and glass chemistry of natural and experimental products: Chemical Geology, v. 483, p. 603–618, https://doi.org/10.1016/j.chemgeo.2018.03.031.

Mbia, P.K., Mortensen, A.K., Oskarsson, N., and Hardarson, B., 2015, Sub-surface geology, petrology and hydrothermal alteration of the Menengai geothermal field, Kenya: case study of wells MW-02, MW-04, MW-06 and MW-07: Proceedings World Geothermal Congress, p. 20.

McIntosh, I.M., Llewellin, E.W., Humphreys, M.C.S., Nichols, A.R.L., Burgisser, A., Schipper, C.I., and Larsen, J.F., 2014, Distribution of dissolved water in magmatic glass records growth and resorption of bubbles: Earth and Planetary Science Letters, v. 401, p. 1–11, https://doi.org/10.1016/j.epsl.2014.05.037.

Mortensen, A.K., Egilson, Þ., Gautason, B., Arnadottir, S., and Gudmundsson, A., 2014, Stratigraphy, alteration mineralogy, permeability and temperature conditions of well IDDP-1, Krafla, NE-Iceland: Geothermics, v. 49, p. 31–41, https://doi.org/10.1016/j.geothermics.2013.09.013.

Mortensen, A.K., Guðmundsson, Á., Steingrímsson, B., Sigmundsson, F., Axelsson, G., Ármannsson, H., Björnsson, H., Ágústsson, K., Sæmundsson, K., Ólafsson, M., Karlsdóttir, R., Halldórsdóttir, S., and Hauksson, T., 2015, The Krafla conceptual model revision—Translation of Report LV-2009/111, *in* Landsvirkjun Report LV-2015-098, 206 p.

Navon, O., and Lyakhovsky, V., 1998, Vesiculation processes in silicic magmas, *in* Gilbert, J.S., and Sparks, R.S.J., eds., The Physics of Explosive Volcanic Eruptions: Geological Society, London, Special Publication 145, p. 27–50, https://doi.org/10.1144/GSL.SP.1996.145.01.03.

Newman, S., Epstein, S., and Stolper, E., 1988, Water, carbon dioxide, and hydrogen isotopes in glasses from the ca. 1340 A.D. eruption of the Mono Craters, California: Constraints on degassing phenomena and initial volatile content: Journal of Volcanology and Geothermal Research, v. 35, p. 75–96, https://doi.org/10.1016/0377-0273(88)90007-8.

Okumura, S., Nakamura, M., and Tsuchiyama, A., 2006, Shear-induced bubble coalescence in rhyolitic melts with low vesicularity: Geophysical Research Letters, v. 33, https://doi.org/10.1029/2006GL027347.

Okumura, S., Nakamura, M., Takeuchi, S., Tsuchiyama, A., Nakano, T., and Uesugi, K., 2009, Magma deformation may induce non-explosive volcanism via degassing through bubble networks: Earth and Planetary Science Letters, v. 281, p. 267–274, https://doi.org/10.1016/j.epsl.2009.02.036.

Pálsson, B., Hólmgeirsson, S., Guðmundsson, Á., Bóasson, H.Á., Ingason, K., Sverrisson, H., and Thórhallsson, S., 2014, Drilling of the well IDDP-1: Geothermics, v. 49, p. 23–30, https://doi.org/10.1016/j.geothermics.2013.08.010.

Pope, E.C., 2011, Hydrogen and oxygen isotope fractionation in hydrous minerals as indicators of fluid source in modern and fossil metasomatic environments [Ph.D. thesis]: Stanford, California, Stanford University, 243 p.

Pope, E.C., Bird, D.K., Arnórsson, S., Fridriksson, T., Elders, W.A., and Friðleifsson, G.O., 2009, Isotopic constraints on ice age fluids in active geothermal systems: Reykjanes, Iceland: Geochimica et Cosmochimica Acta, v. 73, p. 4468–4488, https://doi.org/10.1016/j.gca.2009.03.033.

Pope, E.C., Bird, D.K., and Arnórsson, S., 2014, Stable isotopes of hydrothermal minerals as tracers for geothermal fluids in Iceland: Geothermics, v. 49, p. 99–110, https://doi.org/10.1016/j.geothermics.2013.05.005.

Rhodes, E., Kennedy, B.M., Lavallée, Y., Hornby, A., Edwards, M., and Chigna, G., 2018, Textural insights into the evolving lava dome cycles at Santiaguito lava dome, Guatemala: Frontiers of Earth Science, v. 6, https://doi.org/10.3389/feart.2018.00030.

Rooyakkers, S.M., Stix, J., Berlo, K., and Barker, S.J., 2020, Emplacement of unusual rhyolitic to basaltic ignimbrites during collapse of a basalt-dominated caldera: The Halarauður eruption, Krafla (Iceland): Geological Society of America Bulletin, v. 132, p. 1881–1902, https://doi.org/10.1130/B35450.1.

Rust, A.C., Manga, M., and Cashman, K.V., 2003, Determining flow type, shear rate and shear stress in magmas from bubble shapes and orientations: Journal of Volcanology and Geothermal Research, v. 122, p. 111–132, https://doi.org/10.1016/S0377-0273(02)00487-0.

Sæmundsson, K., 1991, Geology of the Krafla system (in Icelandic), *in* Náttúra Mývatns (The Natural History of Lake Mývatn): Reykjavík, Icelandic Natural History Society, p. 24–95.

Schiffman, P., Zierenberg, R.A., Mortensen, A.K., Frioleifsson, G.O., and Elders, W.A., 2014, High temperature metamorphism in the conductive boundary layer adjacent to a rhyolite intrusion in the Krafla geothermal system, Iceland: Geothermics, v. 49, p. 42–48, https://doi.org/10.1016/j.geothermics.2012.11.002.

Schipper, C.I., Castro, J.M., Kennedy, B.M., Christenson, B.W., Aiuppa, A., Alloway, B., Forte, P., Seropian, G., and Tuffen, H., 2019, Halogen (Cl, F) and sulphur release during explosive, effusive, and intrusive phases of the 2011 rhyolitic eruption at Cordón Caulle volcano (Chile): Volcanica, v. 2, p. 73–90, https://doi.org/10.30909/vol.02.01.7390.

Schuler, J., Greenfield, T., White, R.S., Roecker, S.W., Brandsdóttir, B., Stock, J.M., Tarasewicz, J., Martens, H.R., and Pugh, D., 2015, Seismic imaging of the shallow crust beneath the Krafla central volcano, NE Iceland: Journal of Geophysical Research. Solid Earth, v. 120, p. 7156–7173, https://doi.org/10.1002/2015JB012350.

Seligman, A.N., and Bindeman, I.N., 2019, The $\delta^{18}O$ of primary and secondary waters in hydrous volcanic glass: Journal of Volcanology and Geothermal Research, v. 371, p. 72–85, https://doi.org/10.1016/j.jvolgeores.2018.12.008.

Seligman, A.N., Bindeman, I.N., Watkins, J.M., and Ross, A.M., 2016, Water in volcanic glass: From volcanic degassing to secondary hydration: Geochimica et Cosmochimica Acta, v. 191, p. 216–238, https://doi.org/10.1016/j.gca.2016.07.010.

Seligman, A.N., Bindeman, I., Van Eaton, A., and Hoblitt, R., 2018, Isotopic insights into the degassing and secondary hydration of volcanic glass from the 1980 eruptions of Mount St. Helens: Bulletin of Volcanology, v. 80, p. 37, https://doi.org/10.1007/s00445-018-1212-6.

Shea, T., Houghton, B.F., Gurioli, L., Cashman, K.V., Hammer, J.E., and Hobden, B.J., 2010, Textural studies of vesicles in volcanic rocks: An integrated methodology: Journal of Volcanology and Geothermal Research, v. 190, p. 271–289, https://doi.org/10.1016/j.jvolgeores.2009.12.003.

Sparks, R.S.J., 1978, The dynamics of bubble formation and growth in magmas: A review and analysis: Journal of Volcanology and Geothermal Research, v. 3, p. 1–37, https://doi.org/10.1016/0377-0273(78)90002-1.

Taylor, B.E., 2001, Hydrogen isotope composition of magmatic water: Review of variations due to source, igneous environment, and degassing processes: Abstract V41C-01, presented at 2001 Spring Meeting, AGU, Boston, Massachusetts, 29 May–2 June.

Taylor, B.E., Eichelberger, J.C., and Westrich, H.R., 1983, Hydrogen isotopic evidence of rhyolitic magma degassing during shallow intrusion and eruption: Nature, v. 306, p. 541–545, https://doi.org/10.1038/306541a0.

Teplow, W., Marsh, B., Hulen, J., Spielman, P., Kaleikini, M., Fitch, D., Rickard, W., 2009, Dacite melt at the Puna geothermal venture wellfield, Big Island of Hawaii: Geothermal resources council transactions, v. 33, p. 989–994.

Toramaru, A., 2006, BND (bubble number density) decompression rate meter for explosive volcanic eruptions: Journal of Volcanology and Geothermal Research, v. 154, p. 303–316, https://doi.org/10.1016/j.jvolgeores.2006.03.027.

Toramaru, A., 2014, On the second nucleation of bubbles in magmas under sudden decompression: Earth and Planetary Science Letters, v. 404, p. 190–199, https://doi.org/10.1016/j.epsl.2014.07.035.

Tuffen, H., and Castro, J.M., 2009, The emplacement of an obsidian dyke through thin ice: Hrafntinnuhryggur, Krafla Iceland: Journal of Volcanology and Geothermal Research, v. 185, p. 352–366, https://doi.org/10.1016/j.jvolgeores.2008.10.021.

Downloaded from http://pubs.geoscienceworld.org/gsa/gsabulletin/article-pdf/doi/10.1130/B35598.1/5211391/b35598.pdf
by Univ of California Davis Serials Dept, Robert A. Zierenberg

Trewick, L., 2015, Vesiculation of rhyolite magma in the IDDP-1 borehole at Krafla, Iceland [M.S. thesis]: Lancashire, England, Lancaster University.

Watson, T., 2018, Evolution of magmatic volatiles during drilling into a magma body, Krafla, Iceland [M.S. thesis]: Canterbury, New Zealand, University of Canterbury.

Yoshimura, S., Kuritani, T., Matsumoto, A., and Nakagawa, M., 2019, Fingerprint of silicic magma degassing visualised through chlorine microscopy: Scientific Reports, v. 9, no. 1, p. 1–10, https://doi.org/10.1038/s41598-018-37374-0.

Zakharov, D.O., Bindeman, I.N., Tanaka, R., Friðleifsson, G.Ó., Reed, M.H., and Hampton, R.L., 2019, Triple oxygen isotope systematics as a tracer of fluids in the crust: A study from modern geothermal systems of Iceland: Chemical Geology, v. 530, no. 119312, https://doi.org/10.1016/j.chemgeo.2019.119312.

Zhang, C., Koepke, J., Wang, L.X., Wolff, P.E., Wilke, S., Stechern, A., Almeev, R., and Holtz, F., 2016, A practical method for accurate measurement of trace level fluorine in Mg- and Fe-bearing minerals and glasses using electron probe microanalysis: Geostandards and Geoanalytical Research, v. 40, p. 351–363, https://doi.org/10.1111/j.1751-908X.2015.00390.x.

Zhang, Y., 1999, H_2O in rhyolitic glasses and melts: Measurement, speciation, solubility, and diffusion: Reviews of Geophysics, v. 37, p. 493–516, https://doi.org/10.1029/1999RG900012.

Zierenberg, R.A., Schiffman, P., Barfod, G.H., Lesher, C.E., Marks, N.E., Lowenstern, J.B., Mortensen, A.K., Pope, E.C., Bird, D.K., Reed, M.H., Friðleifsson, G., and Elders, W.A., 2013, Composition and origin of rhyolite melt intersected by drilling in the Krafla geothermal field, Iceland: Contributions to Mineralogy and Petrology, v. 165, p. 327–347, https://doi.org/10.1007/s00410-012-0811-z.

Science Editor: Brad S. Singer
Associate Editor: Jocelyn McPhie

Manuscript Received 20 December 2019
Revised Manuscript Received 2 October 2020
Manuscript Accepted 10 November 2020

Printed in the USA

Downloaded from http://pubs.geoscienceworld.org/gsa/gsabulletin/article-pdf/doi/10.1130/B35598.1/5211391/b35598.pdf
by Univ of California Davis Serials Dept, Robert A. Zierenberg